Unravelling a mechanistic link between mitophagy defect, mitochondrial malfunction, and apoptotic neurodegeneration in MPS VII

Nishan Mandal[#1], Apurba Das[#1], and Rupak Datta[*1]

[1]Department of Biological Sciences, Indian Institute of Science Education and Research (IISER) Kolkata, Mohanpur, West Bengal, INDIA

[#] These authors contributed equally

[*] Author for correspondence:

Rupak Datta

E-mail: rupakdatta@iiserkol.ac.in

Tel: +91 033 6136 0000; Extn: 1214

ORCID identifier: 0000-0003-1820-9251

Summary

Progressive neurodegeneration and cognitive disability are prominent symptoms of MPS VII, a lysosomal storage disorder caused by β-glucuronidase enzyme deficiency. Yet, the mechanism of neurodegeneration in MPS VII remains elusive thereby limiting the scope of targeted intervention. To address this, we recently developed a β-glucuronidase-deficient (CG2135$^{-/-}$) *Drosophila* model of MPS VII. The CG2135$^{-/-}$ flies exhibited signs of neuromuscular degeneration, including loss of dopaminergic neurons, and accumulated engorged lysosomes, ubiquitinated proteins and mitochondria in their brains. These observations, coupled with our current finding that the CG2135$^{-/-}$ flies were highly susceptible to starvation, prompted us to investigate potential defects in the autophagy-lysosomal clearance machinery in the brain. We found that both autophagy induction and lysosome-mediated autophagosomal turnover were impaired in the CG2135$^{-/-}$ fly brain. This was evidenced by lower Atg8a-II levels, reduced Atg1 and Ref(2)P expression along with accumulation of lipofuscin-like inclusions and multilamellar bodies. Interestingly, mitophagy was also found to be defective in their brain, causing buildup of enlarged mitochondria with distorted cristae and reduced membrane potential. This, in turn, affected mitochondrial function as reflected by drastically reduced brain ATP levels. Energy depletion triggered apoptosis in neuronal as well as non-neuronal cells of the CG2135$^{-/-}$ fly brain, where we also detected apoptotic dopaminergic neurons. Resveratrol treatment, previously found to protect against loss of dopaminergic neurons in the CG2135$^{-/-}$ flies, has now been shown act by correcting the mitophagy defect and preventing ATP depletion. Collectively, our study establishes a causal link between mitophagy defect, mitochondrial malfunction, and apoptotic neurodegeneration in MPS VII.

Key words:

MPS VII, autophagy, mitophagy, neurodegeneration, energy depletion, apoptosis, resveratrol

Introduction

Mucopolysaccharidosis VII (MPS VII) is a recessively inherited lysosomal storage disorder caused by mutations in the *β-glucuronidase* (*β-GUS*) gene. β-GUS is one of the eleven glycosaminoglycan (GAG)-catabolizing lysosomal hydrolase, deficiency of which results in accumulation of undegraded or partially degraded GAGs in the lysosomes [1,2]. MPS VII patients suffer from progressive multiorgan dysfunction, and most of them eventually succumb to premature death. Common clinical manifestations of MPS VII include, hydrops fetalis, short stature with coarse face and skeletal deformities, heart valve abnormality, hepato-splenomegaly, and recurrent infections [1–3]. Additionally, MPS VII patients also develop a variety of neurological symptoms like mental retardation, limited vocabulary, delayed speech, hearing impairment and restricted movement [3,4]. This indicates that MPS VII patients suffer from neurodegeneration, which was corroborated by autopsy studies showing extensive lysosomal storage in different regions of the patient's brain [5,6]. The MPS VII mouse model also exhibited accumulation of storage vacuoles throughout the brain and signs of neurodegeneration in the hippocampus and cerebral cortex regions that worsened with age [7]. However, the molecular and cellular events that connect lysosomal storage to neurodegeneration in MPS VII are still not well-understood. Without this knowledge, developing a mechanism-based therapy to ameliorate neurological problems of MPS VII patients remains an unmet need. This issue has become even more critical because enzyme replacement therapy (ERT), the only approved treatment for MPS VII patients, despite being successful in alleviating some of the disease symptoms, has not yet been shown to resolve the neurological complications [8,9]. This is most likely due to the limited ability of the infused enzyme to cross the blood brain barrier [9]. All these challenges emphasize the urgent need for an in-depth study of the brain pathology and the mechanism of neurodegeneration in MPS VII that would facilitate exploration of small molecule-based therapy.

Towards this goal, recently we developed the first *Drosophila* model of MPS VII by knocking-out the fly *β-GUS* gene (*CG2135*) [10]. The CG2135$^{-/-}$ fly exhibited progressive locomotor disability, attributed to neuromuscular degeneration. The CG2135$^{-/-}$ fly brain displayed distinctive features like, extensive vacuolation, abnormal buildup of engorged lysosome as well as ubiquitinated proteins and an increased abundance of MitoTracker-positive vesicles. Interestingly, a significant loss of dopaminergic neurons

84 was also observed in the CG2135$^{-/-}$ fly brain [10]. Dopaminergic neurons are classically known to control
85 locomotion and their depletion is associated with movement disorders such as Parkinson's disease [11,12].
86 These initial findings provided us with an excellent platform for delving deeper into the underlying
87 mechanism of neurodegeneration in MPS VII.

88 In line with our observation in the CG2135$^{-/-}$ fly brain, Martins *et. al.* previously reported mitochondrial
89 accumulation in the MPS IIIC mouse brain. Their data also revealed a progressive decline in activities
90 of some of the respiratory chain enzymes in mitochondria isolated from the MPS IIIC mice brain [13].
91 Apart from these two MPS disorders, mitochondrial accumulation in brain was also reported in animal
92 models of few other unrelated lysosomal storage disorders, e.g. Gaucher disease, multiple sulfatase
93 deficiency and CLN7 [14–16]. In this context, it is worth mentioning that, due to their high energy demand,
94 neuronal cells rely heavily on mitochondrial quality control to maintain a healthy and efficient pool of
95 mitochondria. These quality control mechanisms include biogenesis of mitochondria, their
96 fusion/fission dynamics and selective clearance of damaged mitochondria through the mitophagy
97 pathway [17]. Aberrations in these processes have been reported to play a role in many neurodegenerative
98 diseases [18,19]. However, very little is known about the mechanistic link between mitochondrial quality
99 control in the brain and neurodegeneration associated with MPS disorders in general, and MPS VII in
100 particular.

101 In this study, we systematically investigated the causes and consequences of abnormal buildup of
102 mitochondria in the CG2135$^{-/-}$ fly brain to better understand the mechanism of neurodegeneration in
103 MPS VII. We initially focused on the autophagy-lysosomal clearance pathway in the brain to check if
104 any defect in this machinery led to inefficient turnover of mitochondria. This notion was fuelled by our
105 previously reported observation of aberrant autophagy in the CG2135$^{-/-}$ larvae [20]. A similar defect was
106 also reported in β-GUS deficient chondrocyte cell line [21]. Autophagy is a coordinated cellular waste
107 disposal system in which cell debris is packed into double-membrane autophagosome vesicles and
108 targeted to lysosome for degradation and recycling [22]. The process involves a series of autophagy-related
109 genes (Atg) and proteins which are regulated by various physiological cues [23]. Apart from bulk
110 autophagy, there are specialized forms of autophagy such as ER-phagy or mitophagy, via which

111 damaged cellular organelles are specifically degraded [19,24]. We first suspected a gross autophagy defect
112 in adult CG2135$^{-/-}$ flies when they were found to be highly susceptible to starvation. Following this lead,
113 we confirmed that autophagy is indeed compromised in the CG2135$^{-/-}$ fly brain. Further probing
114 uncovered that the process of mitophagy was also impaired in the CG2135$^{-/-}$ fly brain, resulting in the
115 accumulation of abnormally large mitochondria with deformed cristae structure and decreased
116 membrane potential. Consequently, ATP levels dropped significantly, triggering extensive apoptotic cell
117 death in the CG2135$^{-/-}$ fly brain, including dopaminergic neurons. Treatment with resveratrol, previously
118 shown to prevent loss of dopaminergic neurons in the CG2135$^{-/-}$ flies, has now been found to protect
119 the CG2135$^{-/-}$ fly brain from mitophagy defect and ATP exhaustion. Our findings thus established a
120 mechanistic link between mitophagy defect, mitochondrial malfunction, and apoptotic
121 neurodegeneration in MPS VII.

122 **Results**

123 **Defective autophagy-lysosome clearance system in CG2135$^{-/-}$ fly brain**

124 During initial characterization of the MPSVII fly (CG2135$^{-/-}$), we observed an abnormal accumulation
125 of MitoTracker-positive puncta and ubiquitinated proteins in their brain, indicating a potential defect in
126 the lysosome-mediated cellular clearance system [10]. In a follow-up study, we reported aberrant
127 autophagy in the CG2135$^{-/-}$ larvae [20]. These findings prompted us to analyze the status of autophagy in
128 the adult CG2135$^{-/-}$ fly, specifically in its brain, to better understand the mechanism of
129 neurodegeneration in this fly model. Autophagy pathway is known to be activated as a protective
130 response to nutrient starvation [25]. Studies with various model organisms have established that an
131 autophagy defect results in enhanced susceptibility to starvation [26–28]. Taking cue from these reports, we
132 compared the starvation sensitivity of the adult CG2135$^{-/-}$ flies with their age-matched wild-type
133 counterparts. For this, we took wild type (W^{1118}) and CG2135$^{-/-}$ flies of different age groups (young flies
134 - 4 days old, middle-aged flies - 15 days old and old flies - ≥ 30 days old) and subjected them to a no-
135 food condition. The percentage survivability was analyzed every 12 hours by counting the number of
136 surviving flies (Figure 1A). The survival curves, as well as the mean survival time (MST) under starved
137 condition, clearly showed that the CG2135$^{-/-}$ flies were more susceptible to starvation than the wild type

138 flies at all ages (Figures 1B-1D). This data strongly indicated that the adult CG2135$^{-/-}$ flies could be
139 suffering from an autophagy defect. We then shifted our focus to a detailed analysis of the autophagy
140 status in the CG2135$^{-/-}$ fly brain. For this, we collected the wild type and CG2135$^{-/-}$ flies of different age
141 groups (4-days old to 45-days old) and examined the level of Atg8a, the *Drosophila* homolog of
142 mammalian LC3, in their brains. Atg8a is considered as a reliable marker for autophagy as it gets
143 recruited to autophagosome vesicles in its phosphatidylethanolamine (PE) conjugated form [29].Our
144 western blot data clearly showed a marked reduction in the Atg8a-II levels (the PE-conjugated form of
145 Atg8a that correlates with the autophagosome abundance) in the CG2135$^{-/-}$ fly brain as compared to
146 their wild type counterparts across all age groups. Notably, the differences in brain Atg8a-II levels
147 between the wild type and the CG2135$^{-/-}$ fly progressively increased with age (Figures 2A and 2B).
148 Consistent with this finding, immunofluorescence staining of whole fly brains with an Atg8a antibody
149 showed a significant reduction in the Atg8a-positive autophagic vesicles in 30-days old CG2135$^{-/-}$ fly
150 brain compared to age-matched control (Figures. S1A-F). In this context, it is worth noting that although
151 there was no significant difference in the Atg8a transcript levels between the wild type and the CG2135^{-}
152 $^{/-}$ fly brains, the Atg8a-I protein level (the non-autophagosome bound form of Atg8a) was also found to
153 be reduced in the CG2135$^{-/-}$ fly brains (Figures S1G – S1I). To ascertain the reason behind the reduced
154 abundance of autophagosomes in the CG2135$^{-/-}$ fly brain, we checked the status of the Ref(2)P, the fly
155 homologue of the mammalian autophagic cargo adapter protein p62/SQSTM1 [30]. As evident from our
156 whole-brain immunofluorescence staining and western blot data, the Ref(2)P protein level in the
157 CG2135$^{-/-}$ fly brain was significantly less as compared to the wild type flies of similar age (Figures 2C
158 – 2I). To study if lowering of the Ref(2)P protein level is due to transcriptional downregulation, we
159 analyzed the Ref(2)P mRNA level by RT-qPCR and found reduced by ~ 40% in the CG2135$^{-/-}$ fly brain
160 (Figure 2J). This prompted us to also check the expression of Atg1, one of the important autophagy
161 initiation genes [31]. Interestingly, almost 60% decline in the transcript level of Atg1 was observed in the
162 CG2135$^{-/-}$ fly brain as compared to their age-matched wild type counterparts (Figure 2K). Collectively,
163 these data indicate that a defect in the autophagy induction might be the underlying reason behind the
164 reduced abundance of the autophagosomes in the old CG2135$^{-/-}$ fly brain. We also noticed that in stark
165 contrast to the wild type flies, the optical lobe and midbrain region of the 45-days old CG2135$^{-/-}$ flies

166 exhibited distinctive autofluorescence when imaged in the FITC channel (Figures 2L – 2N). Such
167 autofluorescent puncta are reminiscent of lipofuscin, the storage granules of undegraded lipids and
168 misfolded proteins that accumulate in the lysosomes of postmitotic neurons [32]. Accumulation of
169 lipofuscin is a hallmark of ageing and also has been reported in many neurodegenerative diseases [33–35].
170 This intriguing finding prompted us to further analyze the tissue architecture of the fly brains using high
171 resolution transmission electron microscopy (TEM). Our TEM images revealed that compared to the
172 wild type flies, the CG2135$^{-/-}$ fly brains contained very few double-membrane autophagosome vesicles
173 but instead had an abundance of multilamellar bodies (MLBs) with whorl-like structures (Figures 2O–
174 2S). Abnormal accumulation of MLBs has been observed in a variety of lysosomal storage disorders,
175 resulting from dysfunction of lysosomal hydrolytic activity [34,36,37]. Considering all these findings, it is
176 evident that both autophagy induction and lysosome-mediated autophagosomal clearance were
177 impaired in the CG2135$^{-/-}$ fly brain.

178 **Abnormal accumulation of enlarged and damaged mitochondria in the CG2135$^{-/-}$ fly brain**

179 One of the unexplained pathological features of the CG2135$^{-/-}$ fly brain is the increased accumulation
180 of MitoTracker-stained puncta [10]. Upon further analysis, we noted that in the 30-days old CG2135$^{-/-}$ fly
181 brain there was a significant increase in the MitoTracker staining intensity (by ~ 1.9 folds) as well as
182 the size of the MitoTracker-positive puncta (by ~ 1.3 folds) compared to the wild type fly brain (Figures
183 3A-3F). The level of the mitochondrial protein ATP5A was also significantly elevated in the CG2135$^{-/-}$
184 fly brain, as revealed from our western blot analysis (Figure S2). Taken together, these data indicated
185 an increased abundance of mitochondrial mass in the CG2135$^{-/-}$ fly brain. To gain deeper insights, we
186 next performed ultrastructure analysis of the mitochondria in the 45-days old fly brains using TEM
187 (Figures 3G and 3H). Examination of the TEM images revealed that compared to the wild type fly brain,
188 there was ~ 1.6 folds increase in the average mitochondria size in the CG2135$^{-/-}$ fly brain (0.27 μm^2 vs.
189 0.43 μm^2) (Figure 3I). Percent frequency distribution analysis of the mitochondria size further revealed
190 that the smaller mitochondria (< 0.2 μm^2) were much more abundant in the wild type fly brain compared
191 to their CG2135$^{-/-}$ counterparts (~ 46% in the wild type vs. ~ 17% in the CG2135$^{-/-}$ fly brain). In contrast,
192 the CG2135$^{-/-}$ fly brain had an increased number of enlarged mitochondria of sizes ≥ 0.4 μm^2 (~ 21%

193 in the wild type vs. ~ 44% in the CG2135$^{-/-}$ fly brain). Abundance of intermediate sized mitochondria
194 (0.2 μm^2 - 0.4 μm^2) was also slightly higher in the CG2135$^{-/-}$ fly brain than the wild type (Figure 3J).
195 Aged mitochondria often exhibit distorted cristae structure and are found to be functionally
196 compromised [38]. This prompted us to methodically examine the mitochondrial ultrastructure from the
197 TEM images and categorized them into healthy, intermediate-damaged, and damaged mitochondria
198 based on the integrity of their cristae structure (Figures 3K-3M). Our analysis revealed that in the wild
199 type fly brain, over 70% of the mitochondria were healthy with orderly packed cristae, whereas, the
200 percentage of healthy mitochondria in the CG2135$^{-/-}$ fly brain was only ~ 45%. In contrast, the CG2135^{-}
201 $^{/-}$ fly brain exhibited a higher abundance of the damaged and intermediate-damaged mitochondria
202 compared to their wild type partners (damaged: 30% in the CG2135$^{-/-}$ vs. 14% in the wild type,
203 intermediate damaged: 25% in the CG2135$^{-/-}$ vs. 14% in the wild type) (Figure 3N). Having confirmed
204 the abundance of enlarged and damaged mitochondria in the CG2135$^{-/-}$ fly brain, our next goal was to
205 understand its cause and functional consequences.

206 **Impaired mitophagy in the CG2135$^{-/-}$ fly brain**

207 Mitochondria are particularly susceptible to oxidative damage due to continuous ROS production
208 during cellular respiration. As a cellular cleansing mechanism, the damaged mitochondria are
209 eliminated through the process of mitophagy, a specialized form of autophagy [17,18]. In this context, it is
210 important to note that impairment of mitophagy has been reported in several age-related
211 neurodegenerative diseases [19]. These prior reports, combined with our finding that autophagy is
212 suppressed in the CG2135$^{-/-}$ fly brain, led us to investigate whether these flies also suffer from a
213 mitophagy defect. For this, 45 days old fly brains were co-stained with LysoTracker (green) and
214 MitoTracker (red), and the mitophagy status was analysed by quantifying the extent of colocalization
215 of lysosomes and mitochondria from confocal images. Data presented in Figures 4A-4H clearly shows
216 that, compared to the wild type flies, there was a significantly reduction in the lysosome-mitochondria
217 colocalization in the CG2135$^{-/-}$ fly brain, indicating a mitophagy defect in these flies. This was further
218 corroborated by our TEM images, which showed fewer autophagosome-engulfed mitochondria in the
219 45-day-old CG2135$^{-/-}$ fly brain compared to their wild type counterparts (Figures 4J and 4L). As an

220 alternative approach to analyse mitophagy, we isolated the mitochondria-rich fraction from 45 days old
221 fly brains and checked for the presence of Atg8a -II, an autophagosome-associated protein, in that
222 fraction. Our western blot data showed that the Atg8a -II protein levels in the mitochondria-rich fraction
223 isolated from the CG2135$^{-/-}$ fly brain was significantly lower than in the age-matched wild type flies
224 (Figures 4M-4O). Taken together, our data suggest that impaired mitophagy is the reason behind the
225 accumulation of enlarged and damaged mitochondria in the CG2135$^{-/-}$ fly brain. This prompted us to
226 investigate the mitochondrial function in the CG2135$^{-/-}$ fly brain, particularly in terms of ATP
227 production.

228 **CG2135$^{-/-}$ fly suffers from brain energy deficit**

229 Mitophagy plays a neuroprotective role by maintaining mitochondrial homeostasis, thereby ensuring
230 sufficient ATP supply for proper brain function [39,40]. Since mitochondrial membrane potential (ΔΨm) is
231 a key indicator of functionally active mitochondria and is essential in driving ATP synthesis, we used
232 JC-1 dye to analyse ΔΨm in the mitophagy-deficient 45 days old CG2135$^{-/-}$ fly brain. JC-1 is a lipophilic
233 green fluorescent monomeric dye that accumulates within the mitochondria in a potential-dependant
234 manner and forms aggregates (J-aggregate) shifting its fluorescence property to red. The red-to-green
235 fluorescence ratio of the JC-1 dye is often used to measure to ΔΨm [41]. Compared to the age-matched
236 wild type flies, we observed > 40% reduction in the red-to-green fluorescence ratio in the CG2135$^{-/-}$ fly
237 brain, indicating a significant decrease in ΔΨm in these flies (Figures 5A-5G). Strikingly, the ATP levels
238 in the 45 days old CG2135$^{-/-}$ fly brain was found to be reduced by >50% than in the wild type fly brain
239 (Figure 5H). This data indicates that the older CG2135$^{-/-}$ flies suffer from severe brain energy deficit,
240 which may be the trigger for neurodegeneration in these flies. ATP is produced in the mitochondrial
241 inner membrane by the enzyme ATP synthase, which utilizes the proton gradient across the
242 mitochondrial membrane as the driving force for generating ATP [41]. It has been reported that if ΔΨm is
243 compromised for some reason, ATP synthase reverses its direction acting as an ATP-consuming enzyme
244 to translocate protons from the mitochondrial matrix to the intermembrane space. In such situations, the
245 expression of ATPase Inhibitory Factor 1 (ATPIF1) is upregulated to prevent wasteful ATP expenditure
246 by inhibiting the ATP synthase activity [42]. Consistent with these findings, we observed a significant

upregulation of ATPIF1 transcript level in the 45 days old CG2135$^{-/-}$ fly brain, suggesting that ATP synthase activity is indeed inhibited in these flies, possibly to counteract further depletion of ATP levels (Figure 5I).

Increased apoptosis in the CG2135$^{-/-}$ fly brain

We previously reported prominent signs of neurodegeneration, including loss of dopaminergic neurons, in the CG22135$^{-/-}$ fly brains [10]. However, the mechanism underlying this neurodegeneration is far from clear. Since mitochondrial damage and ATP depletion have been reported to induce apoptotic cell death in both neuronal and non-neuronal cells [43–45], we checked the status of apoptosis in the energy-deficient 45 days old CG2135$^{-/-}$ fly brain. Our western blot data clearly showed that the CG2135$^{-/-}$ fly brains had significantly elevated levels of cleaved-caspase-3, a key mediator of apoptosis (Figures 6A an 6B) [46]. Interestingly, co-immunostaining of the fly brains with antibodies against cleaved-caspase-3 and ELAV (a pan-neuronal marker) [47] revealed that both neuronal (ELAV-positive) as well as non-neuronal (ELAV-negative) cells in the CG2135$^{-/-}$ fly brain showed signs of apoptosis (Figure S3). These findings were corroborated by transcript analysis of the proapoptotic factor Hid[48], which showed ~ 2.4 folds upregulation in the CG2135$^{-/-}$ fly brain compared to their age-matched counterparts (Figure 6C). For direct visualization of DNA fragmentation in apoptotic cells, we next performed TUNEL staining in whole mount brains. We observed ~ 2.8 folds increase in the abundance of TUNEL-positive cells in the 45 days old CG2135$^{-/-}$ fly brains compared to the wild type fly brains (Figures 6D-6L). When the brains were co-stained with anti-Tyrosine Hydroxylase antibody (to mark the dopaminergic neurons) and TUNEL (to mark the apoptotic nuclei), we observed that ~ 18% of the dopaminergic neurons in the CG2135$^{-/-}$ fly brains were TUNEL positive, as compared to only ~ 2% in the wild type flies (Figures 6M-6S). Collectively, these data suggest that apoptosis plays a key role in neurodegeneration in the MPS VII fly.

Resveratrol treatment corrects mitophagy defect and prevents ATP loss in the CG2135$^{-/-}$ fly brain

We previously reported that resveratrol treatment reversed the locomotor deficit in the CG2135$^{-/-}$ fly and protected against loss of their dopaminergic neurons [10]. But how these abnormalities were corrected by resveratrol remained a mystery. To evaluate the mechanism of resveratrol action, we treated the

274 CG2135$^{-/-}$ flies with it for 30-45 days starting from day 4 post-eclosion. We then assessed the status of
275 Atg1 transcript and the level of mitochondrial protein ATP5A in the brain. We found that Atg1 transcript
276 level, which was significantly downregulated in the CG2135$^{-/-}$ fly brain, was completely restored to the
277 normalcy in the resveratrol-treated CG2135$^{-/-}$ flies (Figure 7A). The elevated ATP5A level in the
278 CG2135$^{-/-}$ fly brain was also reduced to the to the basal level upon resveratrol treatment (Figures 7B
279 and 7C). Most importantly, resveratrol treatment protected the CG2135$^{-/-}$ flies from brain energy deficit
280 by completely restoring their ATP levels (Figure 7D). From our data, it can be conjectured that
281 correction of mitophagy defect and restoration of ATP levels in the CG2135$^{-/-}$ fly brain upon resveratrol
282 treatment is the mechanistic basis for its neuroprotective effect.

283 **Discussion**

284 Despite being known as a debilitating disease with prominent neurological symptoms, the mechanism
285 of neurodegeneration in MPS VII remains poorly understood. The work presented here aimed to bridge
286 this knowledge gap by employing a *Drosophila* model of the disease (the CG2135$^{-/-}$ fly). We report a
287 gross defect in the autophagy-lysosome clearance pathway in the CG2135$^{-/-}$ fly brain, which also
288 manifested as impaired mitophagy. As a consequence, there was an accumulation of structurally
289 deformed and functionally compromised mitochondria leading to bioenergy deficit in the brain and
290 apoptotic neurodegeneration. We also demonstrated that mitophagy defect and brain energy deficit in
291 the CG2135$^{-/-}$ fly could be corrected by treatment with resveratrol, providing a potential explanation for
292 its neuroprotective property.

293 Autophagy is crucial for maintaining cellular homeostasis by clearing cytotoxic protein aggregates and
294 damaged organelles, a process especially vital for post-mitotic cells like neurons in the central nervous
295 system (CNS) [22,49]. In fact, defective autophagy has been linked with neurodegenerative diseases like
296 Alzheimer's, Parkinson's, and ALS [49]. Lysosomal storage disorders (LSDs) such as multiple sulfatase
297 deficiency, Gaucher disease and mucolipidosis type IV, often exhibit neurodegeneration in brain with
298 impaired autophagy [14,15,34]. Despite these studies, the status of autophagy in the MPS VII brain remained
299 completely unexplored. Even for other MPS disorders, there is hardly any systematic study on brain
300 autophagy. We, therefore, took up this challenge following the lead from our earlier observation of

301 defective autophagy in the CG2135$^{-/-}$ larvae [20]. Also, in the present study, the adult CG2135$^{-/-}$ flies were
302 found to be highly susceptible to starvation. Since autophagy is typically induced as a survival response
303 under nutrient starvation, this starvation-sensitivity was an indicator of a global autophagy defect in the
304 CG2135$^{-/-}$ flies [26,27]. However, as autophagic response is highly tissue-specific and it is known that
305 starvation-induced autophagy in brain is much less pronounced than in other tissues [50], it was imperative
306 for us to specifically analyze the autophagy status in the adult CG2135$^{-/-}$ fly brains. A significantly
307 reduced abundance of Atg8a-II protein, a bona fide marker of autophagosomes, confirmed that
308 autophagy is indeed altered in the CG2135$^{-/-}$ fly brains. It was interesting to note that the Atg8a-II levels
309 in the wild type fly brains gradually increased with age, indicating normal autophagy induction but
310 progressive decline of lysosome-mediated autophagosome turnover leading to autophagosome
311 accumulation [51,52]. But, the Atg8a-II levels in the CG2135$^{-/-}$ fly brains did not increase with age and
312 remained almost at the basal level throughout. This result, together with our data demonstrating
313 significantly reduced expression of Atg1 and Ref(2)P in the CG2135$^{-/-}$ fly brains, suggest impaired
314 autophagy induction in the MPS VII flies. The process of autophagy is fine-tuned by multilayered
315 regulation of Atg1/ULK1 initiation factor [53]. Various transcription factors (like ATF4, FoxO3, STAT1,
316 and ZKSCAN3) and signal transducers (like mTOR and AMPK) have been shown to regulate the
317 expression and activity of Atg1/ULK1[54,55]. It remains to be seen whether altered expression of any of
318 these regulatory proteins is responsible for downregulation of Atg1 in the CG2135$^{-/-}$ fly brains.
319 Atg1/ULK1, once activated, initiates autophagy by phosphorylating its downstream targets leading to
320 the assembly of Atg12-Atg5-Atg16L1 complex. It acts as a E3 ligase, facilitating lipidation of cytosolic
321 Atg8a-I/LC3-1 to autophagosome-bound Atg8a-II/LC3-II [51]. So, it is not surprising that under the
322 condition of suppressed Atg1 expression, Atg8a-II levels remained consistently low at all ages in the
323 CG2135$^{-/-}$ fly brains. The low transcript as well as protein levels of Ref(2)P in the CG2135$^{-/-}$ fly brains
324 was rather intriguing. Ref(2)P, the fly orthologue of the mammalian autophagic cargo adaptor protein
325 p62, usually accumulates when there is a block in the autophagy pathway [56]. However, a contrasting
326 observation was reported in peripheral blood mononuclear cells (PBMCs) from Gaucher disease
327 patients, where LC3-II levels as well as p62 transcript were both found to be reduced compared to
328 PBMCs from healthy donor [57]. This suggest that Ref(2)P/p62 expression and autophagy induction could

329 be simultaneously impaired under certain conditions, although physiological implication of such
330 phenomenon is not clear. Ref(2)P/p62 being a TFEB-inducible gene, its reduced expression in the
331 CG2135$^{-/-}$ fly brains might be a collateral consequence of TFEB downregulation [58]. While TFEB has
332 been found to be dysregulated in some neurodegenerative diseases [59], its status is not known in any of
333 the MPS disorders and this remains a future area for investigation.

334 In addition to stunted autophagy induction, defective clearance of the autophagosomal content was also
335 evident in the CG2135$^{-/-}$ fly brains, as indicated by accumulation of lipofuscin-like inclusions and
336 multilamellar bodies (MLBs). Lipofuscin is an intralysosomal autofluorescent material mainly
337 composed of lipids and misfolded proteins that are resistant to lysosomal degradation. Lipofuscin
338 accumulation can be aggravated when lysosomal degradation process is hampered, particularly in
339 certain lysosomal storage diseases such as Batten disease, Tay-Sachs disease and Sanfilippo syndrome
340 [33,60,61]. Accumulation of concentric multilamellar structures in the CG2135$^{-/-}$ fly brains is another
341 signature for dysfunctional lysosomal activity, as has been observed in the brains of a *Drosophila* model
342 of mucolipidosis type IV and fibroblasts form Parkinson's disease patients [34,36,62].

343 Autophagy being a critical homeostatic machinery in neuronal as well as some non-neuronal cells of
344 the central nervous system [63–65], blockage in multiple steps of this pathway in the CG2135$^{-/-}$ fly brains
345 was expected to have deleterious consequences. This notion was validated when we found significantly
346 reduced mitochondria-lysosome colocalization and fewer autophagosome-sequestered mitochondria in
347 the CG2135$^{-/-}$ fly brains, indicating a defect in mitophagy, a specialized form of autophagy to remove
348 damaged mitochondria. As the primary site for cellular energy production, mitochondria are prone to
349 oxidative damage [18]. This vulnerability is even more pronounced in high energy-demanding tissues like
350 the brain [66]. To maintain a healthy pool of mitochondria, cells are endowed with a robust mitochondrial
351 quality control mechanism that comprises two opposing but coordinated processes: mitochondrial
352 biogenesis, and removal of damaged mitochondria through mitophagy [17,18]. The canonical mitophagy is
353 mediated by the PINK1-Parkin signalling cascade. In this pathway, PINK1 is stabilized on the
354 mitochondrial outer membrane, following which it phosphorylates and recruits Parkin, thereby
355 triggering ubiquitin-dependent mitophagy [17]. In PINK1-Parkin-independent non-canonical mitophagy,

356 adaptor molecules on the mitochondrial membrane, such as FUNDC1, can directly initiate mitophagy
357 [67,68]. It has been reported that Atg1/ULK1 plays a vital role in regulating mitophagy through both
358 canonical and non-canonical pathways by phosphorylating key molecules like Parkin or FUNDC1 [68–
359 71]. Thus, it can be speculated that reduced Atg1 expression in the CG2135$^{-/-}$ fly brains is responsible, at
360 least in part, for the observed mitophagy defect. Decreased Ref(2)P levels may also contribute to
361 impaired mitophagy, as p62/Ref(2)P downregulation has been shown to cause autophagic cargo loading
362 failure [72]. Furthermore, PINK1-Parkin-mediated mitophagy is reported to depend on p62/Ref(2)P [73],
363 suggesting that reduced levels of this cargo adapter protein could aggravate the mitophagy defect in the
364 CG2135$^{-/-}$ fly brains.

365 The mitophagy defect in the CG2135$^{-/-}$ fly brains provided an explanation for the accumulation of
366 enlarged mitochondria with deformed cristae structure and reduced ΔΨm. It is well-documented that
367 such excessive buildup of damaged mitochondria is a direct consequence of a mitophagy defect,
368 regardless of the actual cause of the defect [74,75]. It is noteworthy that while signs of autophagy defect
369 were evident even in the younger CG2135$^{-/-}$ flies, accumulation of damaged and depolarized
370 mitochondria in their brains could be detected only in the older flies, aged 30 days and beyond. In fact,
371 the brains of 45 days old CG2135$^{-/-}$ flies were found to be bioenergetically inefficient showing nearly a
372 50% drop in ATP levels. Such mitophagy deficiency-induced depletion of ATP levels in the brain has
373 been observed in other neurodegenerative diseases [76,77], but not reported earlier in any of the MPS
374 disorders. Since ΔΨm is a key driver for ATP synthesis [41], it can be inferred that ATP depletion in the
375 CG2135$^{-/-}$ fly brain is primarily due to accumulation of depolarized mitochondria with significantly
376 reduced ATP-synthesizing ability. Consumption of ATP via reversal of ATP synthase activity, as often
377 occurs in depolarized mitochondria [42], may further exhaust the ATP levels in the CG2135$^{-/-}$ fly brains.
378 Robust upregulation of ATPIF1 transcript level in the CG2135$^{-/-}$ fly brains support this possibility.
379 Under conditions of compromised ΔΨm, ATPIF1 is known to act as an inhibitor of ATP synthase
380 activity, preventing ATP wastage [42].

381 Depleted level of intracellular ATP is an established determinant of apoptotic cell death [45,78]. Thus, it
382 was not unexpected that ATP depletion in a high energy-demanding tissue like brain would induce

383 apoptotic cell death in the CG2135$^{-/-}$ flies. Multiple reports have confirmed that autophagy machinery
384 plays a crucial pro-survival role and defects in this process predispose cells to apoptosis [79–81]. Therefore,
385 in addition to ATP depletion, autophagy impairment could be another factor for inducing apoptosis in
386 the CG2135$^{-/-}$ fly brains. Earlier, we reported a significant loss of dopaminergic neurons in the CG2135^{-}
387 $^{/-}$ fly brains, which could be mitigated with resveratrol treatment [10]. However, the underlying cause of
388 this neuronal loss and the mechanism by which resveratrol conferred protection against it remained
389 unclear. The cause of neuronal loss became evident when we discovered that neuronal cells, particularly
390 the dopaminergic neurons, are undergoing apoptosis in the CG2135$^{-/-}$ fly brains. This finding mirrors
391 one of the hallmarks of Parkinson's disease, which is characterized by progressive loss of dopaminergic
392 neurons via apoptosis [82]. It is worth noting that dopaminergic neurons have a high metabolic demand
393 due to their extensive axonal network and dopamine secretory activity, making them particularly
394 vulnerable to energy crisis [83]. Intriguingly, we observed that resveratrol treatment could correct the
395 mitophagy defect and fully restore ATP levels in the CG2135$^{-/-}$ fly brains, providing a mechanistic
396 explanation for its neuroprotective property. These findings align with an earlier report demonstrating
397 that resveratrol provides neuroprotection by safeguarding against rotenone-induced mitochondrial
398 damage through the enhancement of autophagic activity [84].

399 Apart from neuronal cells, signs of apoptosis were also found in some non-neuronal cells of the
400 CG2135$^{-/-}$ fly brains. In *Drosophila* brain, non-neuronal cells are predominantly glial cells, which play
401 crucial roles in maintaining and protecting neural environment [85]. Whether degeneration of glial cells
402 also drives neurodegeneration in MPS VII remains an open question. It has been observed that
403 degenerating glial cells derived from MPS II mice were able to promote neuronal death in a co-culture
404 condition [86]. Given that the role of mitophagy in glial cells has been implicated in the pathogenesis of
405 other neurodegenerative diseases [87,88], it may be worthwhile to investigate the contributions of these
406 cells in neurodegeneration associated with MPS VII and related disorders.

407 To conclude, the work presented here significantly advances our understanding of the pathogenesis of
408 MPS VII by uncovering a previously unknown mechanistic link between mitophagy defect,
409 mitochondrial malfunction leading to brain energy deficits, and apoptotic neurodegeneration. This study

410 also led to the identification of critical molecular alterations in the autophagy-lysosomal pathway in the
411 MPS VII fly brains, which may provide novel therapeutic leads for pharmacological interventions. The
412 promising results with resveratrol treatment in correcting the mitophagy defect and preventing loss of
413 ATP could be an important first step towards this direction. Since MPS disorders share many
414 commonalities, our findings are likely to have broader implications in understanding the mechanisms
415 of neurodegeneration associated with this group of lysosomal storage diseases.

416 **Acknowledgements**

417 This research was supported by the MoE, Govt. of India grant STARS/APR2019/BS/779/FS awarded
418 to RD. The authors express their sincere gratitude to Mohit Prasad and the members of his fly lab for
419 their support in fly maintenance. Thanks are also due to Sankar Maiti, Arnab Gupta, and Jayasri Das
420 Sarma for sharing critical reagents and facilities. The authors acknowledge Sudipta Bar for his valuable
421 suggestions and Subhankar Dolai for his critical comments on the manuscript. Abhrajyoti Nandi, Sujoy
422 Bose and Subhajit Majumdar are appreciated for their technical assistance. The support of the TEM
423 facility at the Institute of Life Sciences (ILS), Bhubaneswar is acknowledged. NM was supported by
424 CSIR fellowship and AD was supported by DBT and ICMR-SRF fellowships.

425 **Author contributions**

426 N.M. A.D. and R.D. conceptualized the work and designed the experiments; N.M. and A.D. performed
427 the experiments; N.M. A.D. and R.D. analysed the data; N.M. A.D. and R.D. wrote the manuscript;
428 R.D. supervised the work and acquired the funding.

429 **Declaration of interests**

430 The authors declare no competing interests

431 **Supplemental information**

432 Figure S1 – S3

433 **Materials and methods**

434 All the reagents are enlisted in the resource table.

435 **Key resource table:**

Reagent or Resource	Source	Identifier
Antibodies		
anti-GABARAP [1:1000 (WB), 1:100 (IF)]	Cell signalling technology	Cat no.: E1J4E
anti-Ref(2)P [1:1000 (WB), 1:500 (IF)]	Abcam	Cat no.: ab178440
Anti-ATP5A [1:10000]	Abcam	Cat no.: ab14748
Anti-cleaved caspase-3 [1:750 (WB), 1:75 (IF)]	Cell signalling technology	Cat no.: 9661
Anti-α-tubulin [1:5000 (WB)]	Biobharati	Cat no.: BB-AB0118
Anti-Elav [1:100]	DSHB	Cat no.: Elav-9F8A9
Anti-tyrosine-hydroxylase [1:500]	Millipore	Cat no.: AB152
Goat Anti-rabbit Alexa-488	Thermo scientific	Cat no.: A11008
Goat Anti-rabbit Alexa-568	Thermo scientific	Cat no.: A11011
Goat Anti-mouse Alexa-488	Thermo scientific	Cat no.: A11001
Goat Anti-mouse Alexa-568	Thermo scientific	Cat no.: A11031
Goat Anti-rabbit I_gG-Peroxidase	Sigma Aldrich	Cat no.: A9169
Goat Anti-mouse I_gG-Peroxidase	Sigma Aldrich	Cat no.: A9044
Chemicals		
Vectashield	Vecta laboratories	Cat no.: H1000
MitoTracker	Invitrogen	Cat no.: M7513
LysoTracker DND green	Invitrogen	Cat no.: L7526
JC1	Invitrogen	Cat no.: T3168
TUNEL	Merck	Cat no.: 12156792910
ATP Determination kit	Invitrogen	Cat no.: A22066
Trizol	Ambion	Cat no.: 15596026
cDNA kit	Thermo scientific	Cat no.: AB1453A
DNase	Thermo scientific	Cat no.: 18068-015
SYBR green	Biorad	Cat no.: 1725121
Protease inhibitor cocktail	Sigma Aldrich	Cat no.: S8830
Triton-X100	Sigma Aldrich	Cat no.: T9284
Tween-20	Sigma Aldrich	Cat no.: 93773
S2 media	Gibco	Cat no.: 21720
FBS	Avantor	Cat no.: 97068-085
Penicillin-streptomycin	Gibco	Cat no.: 10378016
Paraformaldehyde	Sigma Aldrich	Cat no.: P6148

Bovine serum albumin	Sigma Aldrich	Cat no.: A2153
Hoechst	Thermo scientific	Cat no.: H1399
Glutaraldehyde	Sigma Aldrich	Cat no.: G7776
Osmium tetroxide	Sigma Aldrich	Cat no.: 75632
Propylene oxide	Sigma Aldrich	Cat no.: 110205
Embed-812	EMS	Cat no.: 14900
DER736	EMS	Cat no.: 13000
NMA	EMS	Cat no.: 19000
DMP-30	EMS	Cat no.: 13600
Uranyless	EMS	Cat no.: 22409
Super Signal West Pico Chemiluminescent Substrate	Thermo scientific	Cat no.: 34580
Resveratrol	Calbiochem	Cat no.: 554325
Oligonucleotides		
dAtg8aF: CGTCGCAAATATCCAGACCG dAtg8aR: GAAGAAGAGGGCATCCTCGG	IDT	NA
dAtg1F: GCCCAACGAACTGAAGTCCTA dAtg1R: TGGCATGTCAACTGGCGAC	IDT	NA
Ref(2)PF: TTCCAGGAGCGCCAGTTAC Ref(2)PR: CGTGCATATTGCTCTCGCAC	IDT	NA
ATPIF1F: CGTAGCGCATCTCGTCTGTA ATPIF1R: AGCTGCTCCCTTTGCTTCTT	IDT	NA
Hid F: GGTACATCCCAAGCGGAGAG Hid R: GGCCAAAACGAAAACGGTCA	IDT	NA

RP49 F: TCTGATGCCCAACATCGGTT RP49 R: TCTCCTTGCGCTTCTTGGAG	IDT	NA
Experimental models/Strains		
W^{1118}	BDSC	
$CG2135^{-/-}$	Bar *et al*., 2018	NA
Softwares		
Zen lite	Carl Zeiss	Version 3.4.91.00000
Fiji	Software	https://imagej.net/Fiji
Prism8	Software	https://www.graphpad.com/scientific-software/ prism/
LASx	Leica	

EXPERIMENTAL MODEL AND METHOD DETAILS:

Drosophila strains and maintenance

W^{1118} flies were obtained from the Bloomington *Drosophila* Stock Centre at Indiana University, USA. The $CG2135^{-/-}$ fly used in this study was reported earlier from our lab by Bar *et. al.* [10] and was maintained by routine outcrossing. W^{1118} and $CG2135^{-/-}$ flies were maintained in controlled density at 25°C under a 12-hour day and night cycle. The standard cornmeal food (corn flour 75g/L, sugar 80g/L, agar 10g/L, dry yeast 15g/L, and malt extract 30g/L) media was used for raising the flies.

For age-matched flies, flies were allowed to lay eggs after synchronization for 24 hours in a cage setup. Then the freshly hatched larvae were collected in equal numbers in food vials. After 9-10 days the newly eclosed flies were collected and used for respective in the experiments. For all the experiments only male flies were used.

Resveratrol dissolved in 100% ethanol (Merck) was added to liquid cornmeal food at 400 µM concentration as previously reported [10]. Flies were kept in continuous exposure of resveratrol starting at day 4 after eclosion till the day of experiment. Resveratrol containing food vials were replaced with fresh vials every alternative day.

Starvation assay:

453 Flies from W^{1118} and $CG2135^{-/-}$ of 4 days, 15 days, and 30 days old were assayed for their survivability
454 in no food condition. On the day of the experiment, flies in a cohort of 10 were kept in vials including
455 a tissue paper soaked in distilled water to mimic no food condition and maintained under a constant
456 temperature of 25°C with 12 hours dark and light cycle. The number of surviving flies monitored from
457 their mobility was considered alive or dead and recorded every 12 hours. More than 130 flies were
458 analysed for the starvation assay, and the experiment was done independently three times. The
459 percentage of survivability was calculated from the total number of flies and live flies at each time
460 point. To calculate mean survivability average number of flies that survived was determined [89].

461 **Western blot**

462 For western blot, 5-10 fly heads were homogenized in 1x Laemmli's (for 1ml 2X 0.5M Tris-Cl pH 6.8
463 0.312ml, SDS 0.05g, glycerol 0.25ml, 1M DTT 50µl) buffer supplemented with 1x protease inhibitor
464 cocktail and boiled at 100°C for 5 min. An equal volume of the fly lysate was subjected to SDS-PAGE.
465 Gels were transferred for 1 hour and blocked in 5% skim milk in 0.025% TBST. The primary antibody
466 incubation was done at 4°C overnight in respective dilutions of antibodies. The secondary antibodies
467 were incubated after washing for 1.5 hours. After final washing, the blots were developed using Super
468 Signal West Pico Chemiluminescent Substrate and captured using the ChemiDoc imaging system
469 (Biorad). α-Tubulin has been used as a loading control. Densitometric analysis of protein bands was
470 quantified using ImageJ software.

471 **Isolation of mitochondria-rich fraction from fly head**

472 Differential centrifugation was performed to isolate mitochondria from the fly head as described
473 previously [90]. Briefly, 50 fly heads were crushed gently with a mortar pestle (25 strokes) in 1 ml lysis
474 buffer containing 250 mM sucrose, 0.1 mM EDTA and 2 mM EGTA. Homogenate was centrifuged at
475 350g for 3 min to eliminate the tissue debris. The supernatant was centrifuged twice at 1000g to
476 eliminate the nuclear fraction. The mitochondria containing supernatant were centrifuged at 10000g for
477 10 min, the pellet was lysed in 1X Laemmeli's buffer and western blot was performed. All the steps
478 were performed in cold. Fractions were checked for the presence of mitochondrial and cytosolic proteins
479 determined by immunoblotting with ATP5A and GAPDH, respectively.

480 **RNA isolation and qRT-PCR**

481 Total RNA was isolated from 10-20 heads of W^{1118} and $CG2135^{-/-}$ flies using TRIzol reagent following
482 the manufacturer's instruction. 1 µg of RNA was used for DNase treatment and DNA-free RNA was
483 reverse transcribed using a cDNA synthesis kit. Transcript levels of different genes were quantified
484 using this cDNA as the template. Quantitative real-time PCR (qRT-PCR) was performed with SYBR
485 Green PCR reaction mix (BioRad) using the Biorad real-time PCR system. Target gene expression was
486 normalized to RP49 as the reference gene (endogenous control). The results of quantitative real-time
487 PCR were analysed by the comparative threshold cycle (CT) method [91].

488 **Immunostaining and imaging**

489 Adult brains from W^{1118} and $CG2135^{-/-}$ were dissected in S2 media supplemented with 10% FBS, 100
490 U/ml penicillin and 100 µg/ml streptomycin. The brains were fixed in 4% paraformaldehyde (PFA) for
491 30 minutes at room temperature. After fixation, the samples were washed in 0.3% PT (1x PBS + 0.3%
492 triton X-100) and blocked with PBT x GS (0.3% PT+0.5% BSA+ 5% Normal goat serum) for 2 hours.
493 The brains were incubated in primary antibodies at 4°C for 36 hours. Following incubation, the brains
494 were washed 5x with 0.3% PT for 15 minutes under gentle shaking conditions and incubated in
495 secondary antibody for 12 hours at 4°C. The washing steps were repeated and counter-stained with
496 DAPI (1µg/ml). After the final wash for 15 minutes the brains were stored in Vectashield until use in
497 the cold. The mounted brains were imaged in Apotome.2 microscope (Carl Zeiss) or Leica SP8 confocal
498 microscope. The image processing was done using the ZEN blue software from Carl Zeiss and for
499 quantification, ZEN blue software and ImageJ were used. For mean intensity measurement, 15-20
500 stacks from the Z planes were merged as MIP (maximum intensity projection) and the mean was taken
501 from the multiple ROIs for each field using ZEN blue.

502 **MitoTracker, LysoTracker, and JC-I staining**

503 MitoTracker staining for age-matched flies was done after dissecting the brain in S2 media [10]. The
504 samples were incubated in 500 nM MitoTracker for 1 hour and Hoechst (2µg/ml) with gentle shaking.
505 After incubation 2 quick washes were given with S2 media. The brains were mounted in media and

506 imaged immediately in Apotome.2 (Carl Zeiss). The intensity of the MitoTracker per unit (1000 x 1000
507 pixel unit area) area and mitochondrial size were measured using ImageJ software.

508 For MitoTracker and LysoTracker co-staining, brains were dissected in S2 media. Following dissection
509 live brains were incubated with 500 nM MitoTracker in S2 media for 30 minutes with Hoechst (2µg/ml)
510 hour at 25°C with gentle shaking in between. After 30 minutes, fresh Mitotracker along with 100 nM
511 LysoTracker green and Hoechst was added and incubated for further 30 minutes. After incubation, 2
512 quick washes were given to remove the excess stain, followed by mounting in S2. The stained brains
513 were immediately imaged with Apotome.2 40X objective. Colocalization between MitoTracker and
514 LysoTracker was analysed using ImageJ. Single stacks of Z plane were taken and analysed using the
515 JaCoP plugin.

516 For JC1 staining the brains were dissected in S2 media supplemented with 10% FBS. Dissected brains
517 were incubated with 2 µM JC1 in S2+10% FBS for 45 mins. After incubation, the stain was discarded
518 and washed quickly with S2+10% FBS. Washed brains were mounted in S2+10% FBS and imaged
519 immediately using Apotome.2 (Carl Zeiss). The red-to-green ratio was calculated from individual stacks
520 analysed in ImageJ.

521 **TUNEL staining**

522 To determine the mechanism of cell death in W^{1118} and $CG2135^{-/-}$ TUNEL assay was performed [92]. The
523 brains were dissected in PBS and fixed in 4% PFA in 0.1% triton for 30mins. Then the samples were
524 washed 2 times each in 0.1% PT and 0.5% PT for 3 mins. The brains were permeabilized in sodium
525 citrate at 65°C for 30 minutes followed by three washes in 0.5% PT. The samples were incubated with
526 the TUNEL mix at 37°C for 3 hours following the manufacturer's instructions. After three washes with
527 0.1% PT and counter-staining with DAPI, the brains were stored in Vectashield and imaged the next
528 day in Apotome.2 (Carl Zeiss). Images acquired were processed in ZEN. 15-20 Z-stacks were taken for
529 MIP and after threshold set for the samples count of TUNEL positive puncta was determined using
530 ImageJ. The count has been represented per brain.

For co-staining with TH (tyrosine hydroxylase), the dissected brain was first immunostained with anti-TH antibody following the above-mentioned methodology used for the TUNEL staining protocol. The brains were mounted in Vectashield and imaged in 63x oil objective Leica SP8 confocal. TUNEL-positive dopaminergic neurons were analysed and manually counted.

Lipofuscin imaging

Lipofuscin imaging was performed following previously described protocol [93]. Briefly, brains from age-matched flies were dissected in cold phosphate buffer and kept on ice for 20 minutes. Then, they were immediately imaged in Apotome.2 (Carl Zeiss) using the FITC channel (Autofluorescence). The images were processed in ZEN blue. To count the number of autofluorescence bodies, MIP of 15 stacks was taken and the threshold was kept the same for all the samples and analysed in ImageJ.

Tissue preparation and Electron microscopy (TEM)

Briefly, the dissected brains were fixed in 2.5% glutaraldehyde overnight, followed by post-fixation in 1% osmium tetroxide for 6h. The fixed tissues were dehydrated in a gradient of ethanol (30 to 100%) and finally in propylene oxide. Dehydrated tissues were infiltrated with resin (Embed-812 2ml, DER736 8ml, NMA 8.9ml and DMP-30 0.28ml) overnight. The next day, individual samples were embedded in capsule moulds and kept at 60°C for 48 hours to facilitate hardening. The samples were cut into ultra-thin using Leica Ultramicrotome. Sections of 70nm were negatively stained in uranyless. The images were acquired in Jeol JEM 2100Plus at 200 keV. The samples were analysed using ImageJ to determine the size and number of mitochondria and multilamellar bodies.

ATP quantification

Total ATP was quantified using an ATP determination kit. For each set of measurement, 10-15 fly heads were homogenized in 1X PBS supplemented with 1X PIC in cold. Supernatant collected by centrifuging the homogenate at 20000g for 20 min was used to measure ATP. Total ATP quantified following manufacturer protocol using a standard curve generated with known concentrations of ATP. Total ATP content was normalized per µg of total protein.

Statistical analysis

557 All the experiments were done at least three times independently. All statistical analysis were done using
558 GraphPad Prism. p-values ≤ 0.05 were considered statistically significant as indicated by asterisks:
559 $*P \leq 0.05$, $**P \leq 0.01$, and $***P \leq 0.001$.

560 **References**

561 1. Sly, W.S., Quinton, B.A., McAlister, W.H., and Rimoin, D.L. (1973). Beta glucuronidase
562 deficiency: Report of clinical, radiologic, and biochemical features of a new
563 mucopolysaccharidosis. J Pediatr *82*, 249–257. https://doi.org/10.1016/S0022-
564 3476(73)80162-3.

565

566 2. Shipley, J.M., Klinkenberg, M., Wu, B.M., Bachinsky, D.R., Grubb, J.H., and Sly, W.S. (1993).
567 Mutational analysis of a patient with mucopolysaccharidosis type VII, and identification of
568 pseudogenes. Am J Hum Genet *52*, 517.

569

570 3. Montaño, A.M., Lock-Hock, N., Steiner, R.D., Graham, B.H., Szlago, M., Greenstein, R., Pineda,
571 M., Gonzalez-Meneses, A., çoker, M., Bartholomew, D., et al. (2016). Clinical course of sly
572 syndrome (mucopolysaccharidosis type VII). J Med Genet *53*, 403–418.
573 https://doi.org/10.1136/JMEDGENET-2015-103322.

574

575 4. Wallace, S.P., Prutting, C.A., and Gerber, S.E. (1990). Degeneration of speech, language, and
576 hearing in a patient with mucopolysaccharidosis VII. Int J Pediatr Otorhinolaryngol *19*, 97–
577 107. https://doi.org/10.1016/0165-5876(90)90215-D.

578

579 5. Vogler, C., Levy, B., Kyle, J.W., Sly, W., Williamson, J., and Whyte, M. (1994).
580 Mucopolysaccharidosis VII: postmortem biochemical and pathological findings in a young
581 adult with beta-glucuronidase deficiency. Modern Pathology.

582

583 6. Irani, D., Kim, H. -S, El-Hibri, H., Dutton, R. V., Beaudet, A., and Armstrong, D. (1983).
584 Postmortem observations on beta-glucuronidase deficiency presenting as hydrops fetalis. Ann
585 Neurol *14*, 486–490. https://doi.org/10.1002/ANA.410140415.

586

587 7. Levy, B., Galvin, N., Vogler, C., Birkenmeier, E.H., and Sly, W.S. (1996). Neuropathology of
588 murine mucopolysaccharidosis type VII. Acta Neuropathol *92*, 562–568.
589 https://doi.org/10.1007/S004010050562/METRICS.

590

591 8. Harmatz, P., Whitley, C.B., Wang, R.Y., Bauer, M., Song, W., Haller, C., and Kakkis, E. (2018). A
592 novel Blind Start study design to investigate vestronidase alfa for mucopolysaccharidosis VII,

593 an ultra-rare genetic disease. Mol Genet Metab *123*, 488–494.
594 https://doi.org/10.1016/J.YMGME.2018.02.006.

595

596 9. Wang, R.Y., da Silva Franco, J.F., López-Valdez, J., Martins, E., Sutton, V.R., Whitley, C.B., Zhang,
597 L., Cimms, T., Marsden, D., Jurecka, A., et al. (2020). The long-term safety and efficacy of
598 vestronidase alfa, rhGUS enzyme replacement therapy, in subjects with
599 mucopolysaccharidosis VII. Mol Genet Metab *129*, 219–227.
600 https://doi.org/10.1016/J.YMGME.2020.01.003.

601

602 10. Bar, S., Prasad, M., and Datta, R. (2018). Neuromuscular degeneration and locomotor deficit in
603 a Drosophila model of mucopolysaccharidosis VII is attenuated by treatment with resveratrol.
604 Dis Model Mech *11*. https://doi.org/10.1242/DMM.036954.

605

606 11. Zhou, Q.Y., and Palmiter, R.D. (1995). Dopamine-deficient mice are severely hypoactive,
607 adipsic, and aphagic. Cell *83*, 1197–1209. https://doi.org/10.1016/0092-8674(95)90145-0.

608

609 12. Auluck, P.K., Chan, H.Y.E., Trojanowski, J.Q., Lee, V.M.Y., and Bonini, N.M. (2002). Chaperone
610 suppression of α-synuclein toxicity in a Drosophila model for Parkinson's disease. Science
611 (1979) *295*, 865–868.
612 https://doi.org/10.1126/SCIENCE.1067389/SUPPL_FILE/1067389S1_THUMB.GIF.

613

614 13. Martins, C., Hulkova, H., Dridi, L., Dormoy-Raclet, V., Grigoryeva, L., Choi, Y., Langford-Smith,
615 A., Wilkinson, F.L., Ohmi, K., DiCristo, G., et al. (2015). Neuroinflammation, mitochondrial
616 defects and neurodegeneration in mucopolysaccharidosis III type C mouse model. Brain *138*,
617 336. https://doi.org/10.1093/BRAIN/AWU355.

618

619 14. Kinghorn, K.J., Grönke, S., Castillo-Quan, J.I., Woodling, N.S., Li, L., Sirka, E., Gegg, M., Mills, K.,
620 Hardy, J., Bjedov, I., et al. (2016). A Drosophila Model of Neuronopathic Gaucher Disease
621 Demonstrates Lysosomal-Autophagic Defects and Altered mTOR Signalling and Is Functionally
622 Rescued by Rapamycin. The Journal of Neuroscience *36*, 11654.
623 https://doi.org/10.1523/JNEUROSCI.4527-15.2016.

624

625 15. Settembre, C., Fraldi, A., Jahreiss, L., Spampanato, C., Venturi, C., Medina, D., de Pablo, R.,
626 Tacchetti, C., Rubinsztein, D.C., and Ballabio, A. (2008). A block of autophagy in lysosomal
627 storage disorders. Hum Mol Genet *17*, 119–129. https://doi.org/10.1093/HMG/DDM289.

628

629 16. Lopez-Fabuel, I., Garcia-Macia, M., Buondelmonte, C., Burmistrova, O., Bonora, N., Alonso-
630 Batan, P., Morant-Ferrando, B., Vicente-Gutierrez, C., Jimenez-Blasco, D., Quintana-Cabrera,

R., et al. (2022). Aberrant upregulation of the glycolytic enzyme PFKFB3 in CLN7 neuronal ceroid lipofuscinosis. Nat Commun *13*. https://doi.org/10.1038/S41467-022-28191-1.

17. Rugarli, E.I., and Langer, T. (2012). Mitochondrial quality control: A matter of life and death for neurons. EMBO Journal *31*, 1336–1349. https://doi.org/10.1038/EMBOJ.2012.38/ASSET/B98C1CBF-817A-412A-A7BF-0E97278DF16A/ASSETS/GRAPHIC/EMBJ201238-FIG-0004-M.JPG.

18. Seo, A.Y., Joseph, A.M., Dutta, D., Hwang, J.C.Y., Aris, J.P., and Leeuwenburgh, C. (2010). New insights into the role of mitochondria in aging: mitochondrial dynamics and more. J Cell Sci *123*, 2533–2542. https://doi.org/10.1242/JCS.070490.

19. Wang, Y., Liu, N., and Lu, B. (2019). Mechanisms and roles of mitophagy in neurodegenerative diseases. CNS Neurosci Ther *25*, 859. https://doi.org/10.1111/CNS.13140.

20. Basu, I., Bar, S., Prasad, M., and Datta, R. (2022). Adipose deficiency and aberrant autophagy in a Drosophila model of MPS VII is corrected by pharmacological stimulators of mTOR. Biochim Biophys Acta Mol Basis Dis *1868*. https://doi.org/10.1016/J.BBADIS.2022.166399.

21. Bartolomeo, R., Cinque, L., De Leonibus, C., Forrester, A., Salzano, A.C., Monfregola, J., De Gennaro, E., Nusco, E., Azario, I., Lanzara, C., et al. (2017). mTORC1 hyperactivation arrests bone growth in lysosomal storage disorders by suppressing autophagy. J Clin Invest *127*, 3717–3729. https://doi.org/10.1172/JCI94130.

22. Morishita, H., and Mizushima, N. (2019). Diverse cellular roles of autophagy. Annu Rev Cell Dev Biol *35*, 453–475. https://doi.org/10.1146/ANNUREV-CELLBIO-100818-125300/CITE/REFWORKS.

23. Mizushima, N., Yoshimori, T., and Ohsumi, Y. (2011). The role of Atg proteins in autophagosome formation. Annu Rev Cell Dev Biol *27*, 107–132. https://doi.org/10.1146/ANNUREV-CELLBIO-092910-154005.

24. Mochida, K., and Nakatogawa, H. (2022). ER -phagy: selective autophagy of the endoplasmic reticulum . EMBO Rep *23*. https://doi.org/10.15252/EMBR.202255192/ASSET/5503D294-66FB-40A0-B536-6AD10D176ED0/ASSETS/GRAPHIC/EMBR202255192-FIG-0004-M.PNG.

25. Shang, L., Chen, S., Du, F., Li, S., Zhao, L., and Wang, X. (2011). Nutrient starvation elicits an acute autophagic response mediated by Ulk1 dephosphorylation and its subsequent

dissociation from AMPK. Proc Natl Acad Sci U S A *108*, 4788–4793. https://doi.org/10.1073/PNAS.1100844108/-/DCSUPPLEMENTAL/PNAS.1100844108_SI.PDF.

26. Scott, R.C., Schuldiner, O., and Neufeld, T.P. (2004). Role and regulation of starvation-induced autophagy in the Drosophila fat body. Dev Cell *7*, 167–178. https://doi.org/10.1016/J.DEVCEL.2004.07.009.

27. Komatsu, M., Waguri, S., Ueno, T., Iwata, J., Murata, S., Tanida, I., Ezaki, J., Mizushima, N., Ohsumi, Y., Uchiyama, Y., et al. (2005). Impairment of starvation-induced and constitutive autophagy in Atg7-deficient mice. Journal of Cell Biology *169*, 425–434. https://doi.org/10.1083/JCB.200412022.

28. Kang, C., You, N.J., and Avery, L. (2007). Dual roles of autophagy in the survival of Caenorhabditis elegans during starvation. Genes Dev *21*, 2161. https://doi.org/10.1101/GAD.1573107.

29. Mizushima, N., and Yoshimori, T. (2007). How to Interpret LC3 Immunoblotting. Autophagy *3*, 542–545. https://doi.org/10.4161/AUTO.4600.

30. Nezis, I.P., Simonsen, A., Sagona, A.P., Finley, K., Gaumer, S., Contamine, D., Rusten, T.E., Stenmark, H., and Brech, A. (2008). Ref(2)P, the Drosophila melanogaster homologue of mammalian p62, is required for the formation of protein aggregates in adult brain. J Cell Biol *180*, 1065. https://doi.org/10.1083/JCB.200711108.

31. Hurley, J.H., and Young, L.N. (2017). Mechanisms of autophagy initiation. Annu Rev Biochem *86*, 225–244. https://doi.org/10.1146/ANNUREV-BIOCHEM-061516-044820/CITE/REFWORKS.

32. Terman, A., and Brunk, U.T. (2004). Lipofuscin. Int J Biochem Cell Biol *36*, 1400–1404. https://doi.org/10.1016/J.BIOCEL.2003.08.009.

33. Haltia, M. (2003). The neuronal ceroid-lipofuscinoses. J Neuropathol Exp Neurol *62*, 1–13. https://doi.org/10.1093/JNEN/62.1.1.

34. Venkatachalam, K., Long, A.A., Elsaesser, R., Nikolaeva, D., Broadie, K., and Montell, C. (2008). Motor deficit in a Drosophila model of mucolipidosis type IV due to defective clearance of apoptotic cells. Cell *135*, 838–851. https://doi.org/10.1016/J.CELL.2008.09.041.

35. Pan, C., Banerjee, K., Lehmann, G.L., Almeida, D., Hajjar, K.A., Benedicto, I., Jiang, Z., Radu, R.A., Thompson, D.H., Rodriguez-Boulan, E., et al. (2021). Lipofuscin causes atypical necroptosis through lysosomal membrane permeabilization. Proc Natl Acad Sci U S A *118*, e2100122118. https://doi.org/10.1073/PNAS.2100122118/SUPPL_FILE/PNAS.2100122118.SAPP.PDF.

36. Hariri, M., Millane, G., Guimond, M.P., Guay, G., Dennis, J.W., and Nabi, I.R. (2000). Biogenesis of Multilamellar Bodies via Autophagy. Mol Biol Cell *11*, 255. https://doi.org/10.1091/MBC.11.1.255.

37. Cunningham, K.M., Maulding, K., Ruan, K., Senturk, M., Grima, J.C., Sung, H., Zuo, Z., Song, H., Gao, J., Dubey, S., et al. (2020). Tfeb/mitf links impaired nuclear import to autophagolysosomal dysfunction in c9-als. Elife *9*, 1–35. https://doi.org/10.7554/ELIFE.59419.

38. Brandt, T., Mourier, A., Tain, L.S., Partridge, L., Larsson, N.G., and Kühlbrandt, W. (2017). Changes of mitochondrial ultrastructure and function during ageing in mice and Drosophila. Elife *6*. https://doi.org/10.7554/ELIFE.24662.

39. Lou, G., Palikaras, K., Lautrup, S., Scheibye-Knudsen, M., Tavernarakis, N., and Fang, E.F. (2020). Mitophagy and Neuroprotection. Trends Mol Med *26*, 8–20. https://doi.org/10.1016/J.MOLMED.2019.07.002.

40. Han, S., Zhang, M., Jeong, Y.Y., Margolis, D.J., and Cai, Q. (2021). The role of mitophagy in the regulation of mitochondrial energetic status in neurons. Autophagy *17*, 4182. https://doi.org/10.1080/15548627.2021.1907167.

41. Zorova, L.D., Popkov, V.A., Plotnikov, E.Y., Silachev, D.N., Pevzner, I.B., Jankauskas, S.S., Babenko, V.A., Zorov, S.D., Balakireva, A. V., Juhaszova, M., et al. (2018). Mitochondrial membrane potential. Anal Biochem *552*, 50–59. https://doi.org/10.1016/J.AB.2017.07.009.

42. Gledhill, J.R., Montgomery, M.G., Leslie, A.G.W., and Walker, J.E. (2007). How the regulatory protein, IF(1), inhibits F(1)-ATPase from bovine mitochondria. Proc Natl Acad Sci U S A *104*, 15671–15676. https://doi.org/10.1073/PNAS.0707326104.

43. Li, S., Zhang, J., Liu, C., Wang, Q., Yan, J., Hui, L., Jia, Q., Shan, H., Tao, L., and Zhang, M. (2021). The Role of Mitophagy in Regulating Cell Death. Oxid Med Cell Longev *2021*. https://doi.org/10.1155/2021/6617256.

44. Pathak, D., Berthet, A., and Nakamura, K. (2013). Energy Failure: Does It Contribute to Neurodegeneration? Ann Neurol *74*, 506. https://doi.org/10.1002/ANA.24014.

45. Lieberthal, W., Menza, S.A., and Levine, J.S. (1998). Graded ATP depletion can cause necrosis or apoptosis of cultured mouse proximal tubular cells. Am J Physiol *274*. https://doi.org/10.1152/AJPRENAL.1998.274.2.F315.

46. Porter, A.G., and Jänicke, R.U. (1999). Emerging roles of caspase-3 in apoptosis. Cell Death Differ *6*, 99–104. https://doi.org/10.1038/SJ.CDD.4400476.

47. Koushika, S.P., Lisbin, M.J., and White, K. (1996). ELAV, a Drosophila neuron-specific protein, mediates the generation of an alternatively spliced neural protein isoform. Curr Biol *6*, 1634–1641. https://doi.org/10.1016/S0960-9822(02)70787-2.

48. Goyal, L., McCall, K., Agapite, J., Hartwieg, E., and Steller, H. (2000). Induction of apoptosis by Drosophila reaper, hid and grim through inhibition of IAP function. EMBO J *19*, 589. https://doi.org/10.1093/EMBOJ/19.4.589.

49. Menzies, F.M., Fleming, A., Caricasole, A., Bento, C.F., Andrews, S.P., Ashkenazi, A., Füllgrabe, J., Jackson, A., Jimenez Sanchez, M., Karabiyik, C., et al. (2017). Autophagy and Neurodegeneration: Pathogenic Mechanisms and Therapeutic Opportunities. Neuron *93*, 1015–1034. https://doi.org/10.1016/J.NEURON.2017.01.022.

50. Mizushima, N., Yamamoto, A., Matsui, M., Yoshimori, T., and Ohsumi, Y. (2004). In vivo analysis of autophagy in response to nutrient starvation using transgenic mice expressing a fluorescent autophagosome marker. Mol Biol Cell *15*, 1101–1111. https://doi.org/10.1091/MBC.E03-09-0704.

51. Rubinsztein, D.C., Mariño, G., and Kroemer, G. (2011). Autophagy and aging. Cell *146*, 682–695. https://doi.org/10.1016/J.CELL.2011.07.030.

52. Chang, J.T., Kumsta, C., Hellman, A.B., Adams, L.M., and Hansen, M. (2017). Spatiotemporal regulation of autophagy during Caenorhabditis elegans aging. Elife *6*. https://doi.org/10.7554/ELIFE.18459.

53. Schreiber, A., Collins, B.C., Davis, C., Enchev, R.I., Sedra, A., D'Antuono, R., Aebersold, R., and Peter, M. (2021). Multilayered regulation of autophagy by the Atg1 kinase orchestrates spatial

and temporal control of autophagosome formation. Mol Cell *81*, 5066-5081.e10. https://doi.org/10.1016/J.MOLCEL.2021.10.024.

54. Zou, L., Liao, M., Zhen, Y., Zhu, S., Chen, X., Zhang, J., Hao, Y., and Liu, B. (2022). Autophagy and beyond: Unraveling the complexity of UNC-51-like kinase 1 (ULK1) from biological functions to therapeutic implications. Acta Pharm Sin B *12*, 3743–3782. https://doi.org/10.1016/J.APSB.2022.06.004.

55. Kim, J., Kundu, M., Viollet, B., and Guan, K.L. (2011). AMPK and mTOR regulate autophagy through direct phosphorylation of Ulk1. Nature Cell Biology 2011 13:2 *13*, 132–141. https://doi.org/10.1038/ncb2152.

56. Sánchez-Martın, P., and Komatsu, M. (2018). p62/SQSTM1 - steering the cell through health and disease. J Cell Sci *131*. https://doi.org/10.1242/JCS.222836.

57. Ivanova, M.M., Changsila, E., Iaonou, C., and Goker-Alpan, O. (2019). Impaired autophagic and mitochondrial functions are partially restored by ERT in Gaucher and Fabry diseases. PLoS One *14*. https://doi.org/10.1371/JOURNAL.PONE.0210617.

58. Settembre, C., Di Malta, C., Polito, V.A., Arencibia, M.G., Vetrini, F., Erdin, S., Erdin, S.U., Huynh, T., Medina, D., Colella, P., et al. (2011). TFEB links autophagy to lysosomal biogenesis. Science *332*, 1429–1433. https://doi.org/10.1126/SCIENCE.1204592.

59. Cortes, C.J., and La Spada, A.R. (2019). TFEB dysregulation as a driver of autophagy dysfunction in neurodegenerative disease: Molecular mechanisms, cellular processes, and emerging therapeutic opportunities. Neurobiol Dis *122*, 83–93. https://doi.org/10.1016/J.NBD.2018.05.012.

60. Toro, C., Zainab, M., and Tifft, C.J. (2021). The GM2 gangliosidoses: Unlocking the mysteries of pathogenesis and treatment. Neurosci Lett *764*. https://doi.org/10.1016/J.NEULET.2021.136195.

61. Oldfors, A., and Sourander, P. (1981). Storage of lipofuscin in neurons in mucopolysaccharidosis - Report on a case of Sanfilippo's syndrome with histochemical and electron-microscopic findings. Acta Neuropathol *54*, 287–292. https://doi.org/10.1007/BF00697002/METRICS.

62. García-Sanz, P., Orgaz, L., Bueno-Gil, G., Espadas, I., Rodríguez-Traver, E., Kulisevsky, J., Gutierrez, A., Dávila, J.C., González-Polo, R.A., Fuentes, J.M., et al. (2017). N370S-GBA1 mutation causes lysosomal cholesterol accumulation in Parkinson's disease. Movement Disorders *32*, 1409–1422. https://doi.org/10.1002/MDS.27119.

63. Komatsu, M., Waguri, S., Chiba, T., Murata, S., Iwata, J.I., Tanida, I., Ueno, T., Koike, M., Uchiyama, Y., Kominami, E., et al. (2006). Loss of autophagy in the central nervous system causes neurodegeneration in mice. Nature 2006 441:7095 *441*, 880–884. https://doi.org/10.1038/nature04723.

64. Choi, I., Wang, M., Yoo, S., Xu, P., Seegobin, S.P., Li, X., Han, X., Wang, Q., Peng, J., Zhang, B., et al. (2023). Autophagy enables microglia to engage amyloid plaques and prevents microglial senescence. Nature Cell Biology 2023 25:7 *25*, 963–974. https://doi.org/10.1038/s41556-023-01158-0.

65. Nixon, R.A., and Rubinsztein, D.C. (2024). Mechanisms of autophagy–lysosome dysfunction in neurodegenerative diseases. Nature Reviews Molecular Cell Biology 2024, 1–21. https://doi.org/10.1038/s41580-024-00757-5.

66. Padamsey, Z., and Rochefort, N.L. (2023). Paying the brain's energy bill. Curr Opin Neurobiol *78*, 102668. https://doi.org/10.1016/J.CONB.2022.102668.

67. Palikaras, K., Lionaki, E., and Tavernarakis, N. (2018). Mechanisms of mitophagy in cellular homeostasis, physiology and pathology. Nature Cell Biology 2018 20:9 *20*, 1013–1022. https://doi.org/10.1038/s41556-018-0176-2.

68. Ham, S.J., Lee, D., Xu, W.J., Cho, E., Choi, S., Min, S., Park, S., and Chung, J. (2021). Loss of UCHL1 rescues the defects related to Parkinson's disease by suppressing glycolysis. Sci Adv *7*. https://doi.org/10.1126/SCIADV.ABG4574/SUPPL_FILE/ABG4574_SM.PDF.

69. Egan, D.F., Shackelford, D.B., Mihaylova, M.M., Gelino, S., Kohnz, R.A., Mair, W., Vasquez, D.S., Joshi, A., Gwinn, D.M., Taylor, R., et al. (2011). Phosphorylation of ULK1 (hATG1) by AMP-activated protein kinase connects energy sensing to mitophagy. Science *331*, 456. https://doi.org/10.1126/SCIENCE.1196371.

70. Hung, C.M., Lombardo, P.S., Malik, N., Brun, S.N., Hellberg, K., Van Nostrand, J.L., Garcia, D., Baumgart, J., Diffenderfer, K., Asara, J.M., et al. (2021). AMPK/ULK1-mediated phosphorylation of Parkin ACT domain mediates an early step in mitophagy. Sci Adv *7*. https://doi.org/10.1126/SCIADV.ABG4544.

71. Wu, W., Tian, W., Hu, Z., Chen, G., Huang, L., Li, W., Zhang, X., Xue, P., Zhou, C., Liu, L., et al. (2014). ULK1 translocates to mitochondria and phosphorylates FUNDC1 to regulate mitophagy. EMBO Rep *15*, 566. https://doi.org/10.1002/EMBR.201438501.

72. Chen, S., Zhou, L., Zhang, Y., Leng, Y., Pei, X.-Y., Lin, H., Jones, R., Orlowski, R.Z., Dai, Y., and Grant, S. (2014). Targeting SQSTM1/p62 induces cargo loading failure and converts autophagy to apoptosis via NBK/Bik. Mol Cell Biol *34*, 3435–3449. https://doi.org/10.1128/MCB.01383-13.

73. Geisler, S., Holmström, K.M., Skujat, D., Fiesel, F.C., Rothfuss, O.C., Kahle, P.J., and Springer, W. (2010). PINK1/Parkin-mediated mitophagy is dependent on VDAC1 and p62/SQSTM1. Nat Cell Biol *12*, 119–131. https://doi.org/10.1038/NCB2012.

74. Chen, Y., and Dorn, G.W. (2013). PINK1- Phosphorylated Mitofusin 2 is a Parkin Receptor for Culling Damaged Mitochondria. Science *340*, 471. https://doi.org/10.1126/SCIENCE.1231031.

75. Hwang, S., Disatnik, M.-H., and Mochly-Rosen, D. (2015). Impaired GAPDH-induced mitophagy contributes to the pathology of Huntington's disease. EMBO Mol Med *7*, 1307. https://doi.org/10.15252/EMMM.201505256.

76. Yu, W., Gong, J.S., Ko, M., Garver, W.S., Yanagisawa, K., and Michikawa, M. (2005). Altered cholesterol metabolism in Niemann-Pick type C1 mouse brains affects mitochondrial function. J Biol Chem *280*, 11731–11739. https://doi.org/10.1074/JBC.M412898200.

77. Bosch, M.E., and Kielian, T. (2019). Astrocytes in juvenile neuronal ceroid lipofuscinosis (CLN3) display metabolic and calcium signaling abnormalities. J Neurochem *148*, 612–624. https://doi.org/10.1111/JNC.14545.

78. Feldenberg, L.R., Thevananther, S., Del Rio, M., De Leon, M., and Devarajan, P. (1999). Partial ATP depletion induces Fas- and caspase-mediated apoptosis in MDCK cells. Am J Physiol Renal Physiol *276*. https://doi.org/10.1152/AJPRENAL.1999.276.6.F837/ASSET/IMAGES/LARGE/AFLU20602007W.JPEG.

79. Levine, B., and Kroemer, G. (2008). Autophagy in the Pathogenesis of Disease. Cell *132*, 27. https://doi.org/10.1016/J.CELL.2007.12.018.

80. Ravikumar, B., Vacher, C., Berger, Z., Davies, J.E., Luo, S., Oroz, L.G., Scaravilli, F., Easton, D.F., Duden, R., and O'kane, C.J. (2006). Rapamycin pre-treatment protects against apoptosis. Hum Mol Genet *15*, 1209–1216. https://doi.org/10.1093/HMG/DDL036.

81. Boya, P., González-Polo, R.-A., Casares, N., Perfettini, J.-L., Dessen, P., Larochette, N., Métivier, D., Meley, D., Souquere, S., Yoshimori, T., et al. (2005). Inhibition of macroautophagy triggers apoptosis. Mol Cell Biol *25*, 1025–1040. https://doi.org/10.1128/MCB.25.3.1025-1040.2005.

82. Venderova, K., and Park, D.S. (2012). Programmed Cell Death in Parkinson's Disease. Cold Spring Harb Perspect Med *2*. https://doi.org/10.1101/CSHPERSPECT.A009365.

83. Surmeier, D.J., Obeso, J.A., and Halliday, G.M. (2017). Selective neuronal vulnerability in Parkinson disease. Nat Rev Neurosci *18*, 101–113. https://doi.org/10.1038/NRN.2016.178.

84. Lin, K.L., Lin, K.J., Wang, P.W., Chuang, J.H., Lin, H.Y., Chen, S. Der, Chuang, Y.C., Huang, S.T., Tiao, M.M., Chen, J.B., et al. (2018). Resveratrol provides neuroprotective effects through modulation of mitochondrial dynamics and ERK1/2 regulated autophagy. Free Radic Res *52*, 1371–1386. https://doi.org/10.1080/10715762.2018.1489128.

85. Stork, T., Bernardos, R., and Freeman, M.R. (2012). Analysis of Glial Cell Development and Function in Drosophila. Cold Spring Harb Protoc *2012*, 1. https://doi.org/10.1101/PDB.TOP067587.

86. Zalfa, C., Verpelli, C., D'avanzo, F., Tomanin, R., Vicidomini, C., Cajola, L., Manara, R., Sala, C., Scarpa, M., Vescovi, A.L., et al. (2016). Glial degeneration with oxidative damage drives neuronal demise in MPSII disease. Cell Death Dis *7*, e2331. https://doi.org/10.1038/CDDIS.2016.231.

87. Morales, I., Sanchez, A., Puertas-Avendaño, R., Rodriguez-Sabate, C., Perez-Barreto, A., and Rodriguez, M. (2020). Neuroglial transmitophagy and Parkinson's disease. Glia *68*, 2277–2299. https://doi.org/10.1002/GLIA.23839.

88. Lautrup, S., Lou, G., Aman, Y., Nilsen, H., Tao, J., and Fang, E.F. (2019). Microglial mitophagy mitigates neuroinflammation in Alzheimer's disease. Neurochem Int *129*, 104469. https://doi.org/10.1016/J.NEUINT.2019.104469.

89. Lushchak, O. V., Gospodaryov, D. V., Rovenko, B.M., Glovyak, A.D., Yurkevych, I.S., Klyuba, V.P., Shcherbij, M. V., and Lushchak, V.I. (2012). Balance between macronutrients affects life span

932 and functional senescence in fruit fly Drosophila melanogaster. J Gerontol A Biol Sci Med Sci
933 *67*, 118–125. https://doi.org/10.1093/GERONA/GLR184.

934

935 90. Rana, A., Oliveira, M.P., Khamoui, A. V., Aparicio, R., Rera, M., Rossiter, H.B., and Walker, D.W.
936 (2017). Promoting Drp1-mediated mitochondrial fission in midlife prolongs healthy lifespan of
937 Drosophila melanogaster. Nat Commun *8*. https://doi.org/10.1038/S41467-017-00525-4.

938

939 91. Livak, K.J., and Schmittgen, T.D. (2001). Analysis of relative gene expression data using real-
940 time quantitative PCR and the 2(-Delta Delta C(T)) Method. Methods *25*, 402–408.
941 https://doi.org/10.1006/METH.2001.1262.

942

943 92. Denton, D., Mills, K., and Kumar, S. (2008). Methods and protocols for studying cell death in
944 Drosophila. Methods Enzymol *446*, 17–37. https://doi.org/10.1016/S0076-6879(08)01602-9.

945

946 93. Hebbar, S., Khandelwal, A., Jayashree, R., Hindle, S.J., Chiang, Y.N., Yew, J.Y., Sweeney, S.T., and
947 Schwudke, D. (2017). Lipid metabolic perturbation is an early-onset phenotype in adult
948 spinster mutants: a Drosophila model for lysosomal storage disorders. Mol Biol Cell *28*, 3728–
949 3740. https://doi.org/10.1091/MBC.E16-09-0674.

950

951

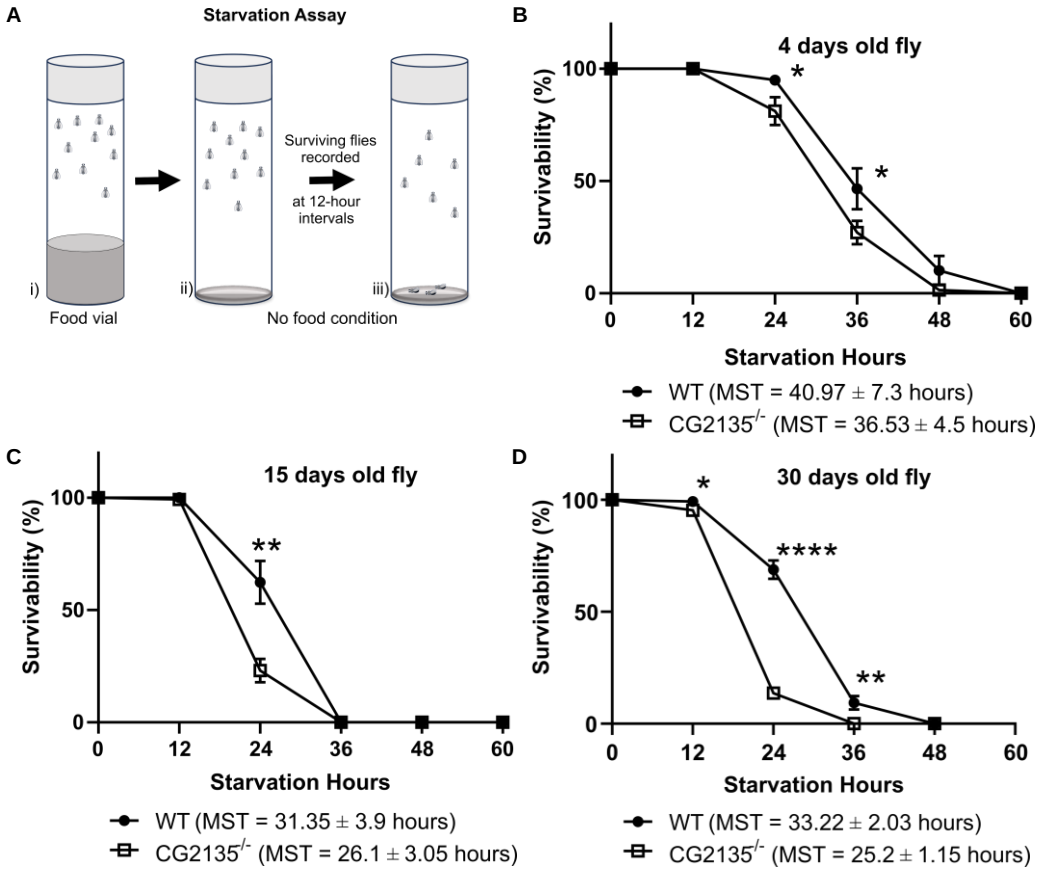

Figure 1: **CG2135$^{-/-}$ flies are significantly more susceptible to starvation**

(A) Schematic representation of experimental setup for starvation assay.

(B-D) Wild type (WT) and CG2135$^{-/-}$ flies of different ages, as indicated in the figure, were subjected to starvation for varying duration and survival curves were plotted. The filled circles and empty squares represent WT the CG2135$^{-/-}$, respectively. Mean survivability time (MST) are mentioned at the bottom of each curve. The survival curves as well as the MST values indicate that the CG2135$^{-/-}$ flies were significantly more susceptible to starvation than their wild type counterparts. All experiments were done independently (N=3), total flies analysed: n≥130.

Error bars represent the standard error of mean (SEM). MST means mean survivability time (hours). Asterisks represent level of significance (****$P \leq 0.0001$, **$P \leq 0.01$, *$P \leq 0.05$; Student's *t*-test).

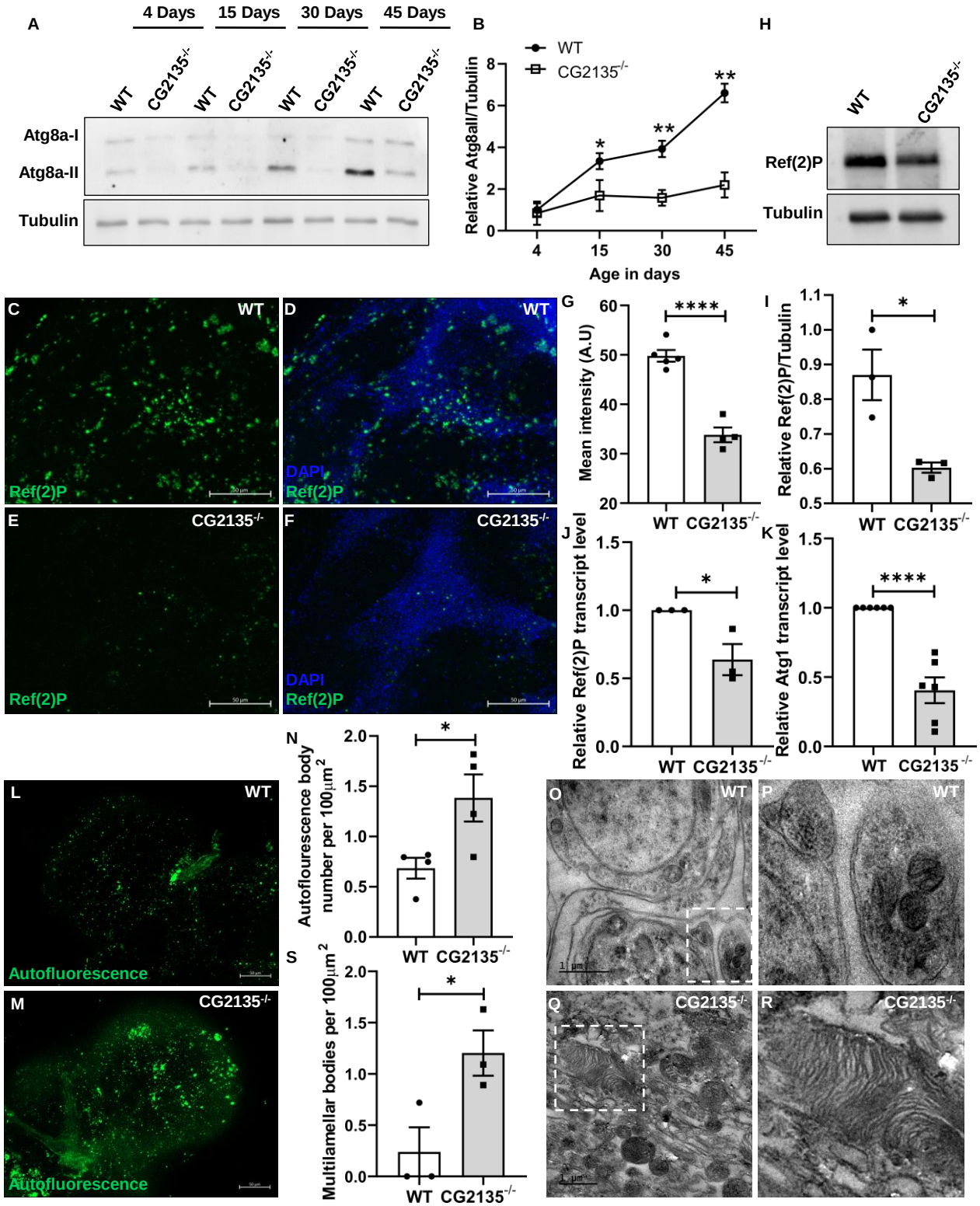
A
4 Days
15 Days
30 Days
45 Days
WT
CG2135-/-
Atg8a-I
Atg8a-II
Tubulin
B
WT
CG2135-/-
Relative Atg8aII/Tubulin
Age in days
H
Ref(2)P
Tubulin
C
D
E
F
Ref(2)P
DAPI
G
Mean intensity (A.U)
I
Relative Ref(2)P/Tubulin
J
Relative Ref(2)P transcript level
K
Relative Atg1 transcript level
L
M
Autofluorescence
N
Autoflourescence body number per 100μm2
S
Multilamellar bodies per 100μm2
O
P
Q
R

Figure 2: Defective autophagy-lysosome clearance machinery in the CG2135$^{-/-}$ fly brain

(A) Western blot of Atg8a showing the protein level of Atg8a-II (14 kDa) from head lysate of wild type (WT) and CG2135$^{-/-}$ of different ages, as indicated in the figure. α-Tubulin (54 kDa) was used as loading control.

(B) The graph represents quantification for Atg8a-II/Tubulin band intensity showing reduced level of Atg8a-II in the CG2135$^{-/-}$ head lysate. (N=3)

(C-F) Immunostaining of Ref(2)P in the 30 days old mid-brain of WT and CG2135$^{-/-}$ with anti-Ref(2)P (green) showing reduced Ref(2)P aggregates in the CG2135$^{-/-}$ brain. Nucleus was counterstained with DAPI (blue).

(G) The bar graph depicting mean fluorescence intensity of Ref(2)P of WT and CG2135$^{-/-}$ brain (N≥4 fly).

(H) Western blot of Ref(2)P (100 kDa) using anti-Ref(2)P from 30 days old WT and CG2135$^{-/-}$ head lysate showing reduced level of the protein in CG2135$^{-/-}$. α-Tubulin (54 kDa) was use as loading control.

(I) The bar graph showing the relative level of Ref(2)P/Tubulin protein (N=3).

(J) Ref(2)P transcript level in 30 days old WT and CG2135$^{-/-}$ fly head was determined by RT-qPCR and normalised to RP49 as housekeeping gene control. (N=3)

(K) Atg1 transcript levels in 30 days old WT and CG2135$^{-/-}$ fly head was determined by RT-qPCR and normalised to RP49 as housekeeping gene control. (N=6)

(L-M) Autofluorescent bodies (detected using the FITC channel) in 45 days old WT and CG2135$^{-/-}$ brain showing an increased autofluorescence in CG2135$^{-/-}$.

(N) Bar graph depicting mean autofluorescence intensity of WT and CG2135$^{-/-}$ brain (N=4).

(O-R) Electron micrograph showing autophagosome and multilamellar bodies from 45 days old WT and CG2135$^{-/-}$ brain. P and R represents magnified images from the respective insets.

(S) Quantification of the number of multilamellar bodies compared between WT and CG2135$^{-/-}$ brain has been represented as a bar graph. Multiple fields were analysed from 3 brains of each genotype. The CG2135$^{-/-}$ had increased number of multilamellar bodies.

All experiments were done independently. Error bars represent the standard error of mean (SEM). Asterisks represent a level of significance (****$P \leq 0.0001$, **$P \leq 0.01$, *$P \leq 0.05$; Student's *t*-test).

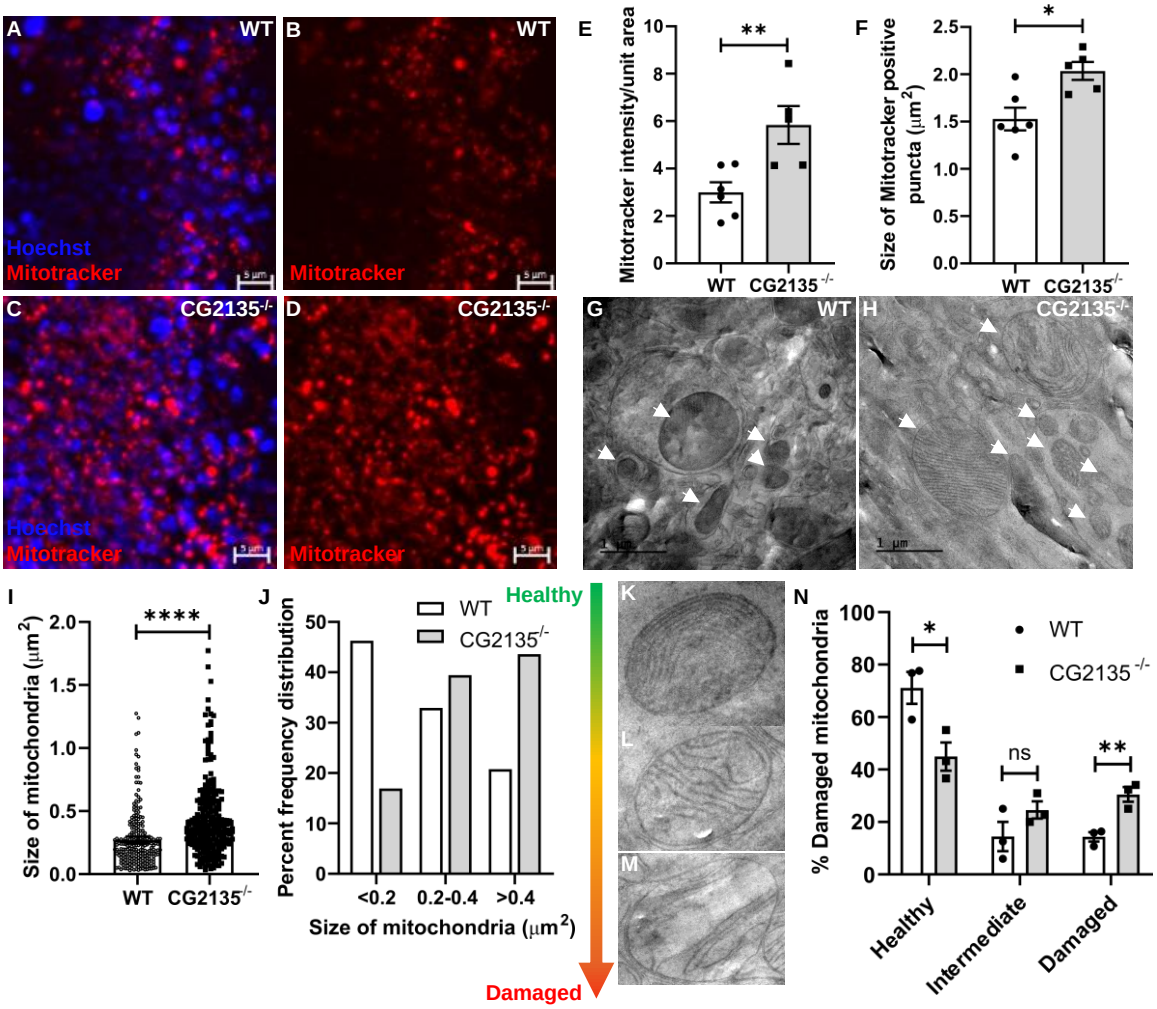

Figure 3: Accumulation of enlarged and damaged mitochondria in the CG2135$^{-/-}$ fly brain

(A-D) Optic lobes of 30 days old wild type (WT) and CG2135$^{-/-}$ fly brain stained with MitoTracker red (showing mitochondria in red) and Hoechst (marking the nucleus in blue), indicating mitochondrial accumulation CG2135$^{-/-}$ fly brain.

(E-F) Quantification of MitoTracker intensity and the size of the MitoTracker positive puncta showing increased mitochondrial mass and puncta size in CG2135$^{-/-}$ fly brain (N ≥ 5 fly brain).

(G-H) Electron micrographs of 45 days old WT and CG2135$^{-/-}$ fly brains. The mitochondria are marked with white arrows are showing the increased number of mitochondria can be seen in CG2135$^{-/-}$ brain.

(I-J) Quantification of the individual mitochondrial area and percent frequency distribution of different sizes showing abundance of larger mitochondria in the CG2135$^{-/-}$ fly brain (N=276 mitochondria from 3 independent experiments) compared to age-matched WT fly brain (N=245 mitochondria from 3 independent experiments). Multiple fields were analysed for measuring the size of the mitochondria using ImageJ.

(K-M) Mitochondria observed under TEM were categorized as healthy (K), intermediate (L), and completely damaged (M) based on their cristae structure.

(N) The percentage of healthy, intermediate-damaged, and completely damaged mitochondria was quantified from multiple fields of 3 independent experiments, showing reduced healthy but increased damaged mitochondria in the CG2135$^{-/-}$ brain.

All experiments were done independently. Error bars represent the standard error of mean (SEM). Asterisks represent a level of significance (****$P \leq 0.0001$, **$P \leq 0.01$, *$P \leq 0.05$; Student's *t*-test).

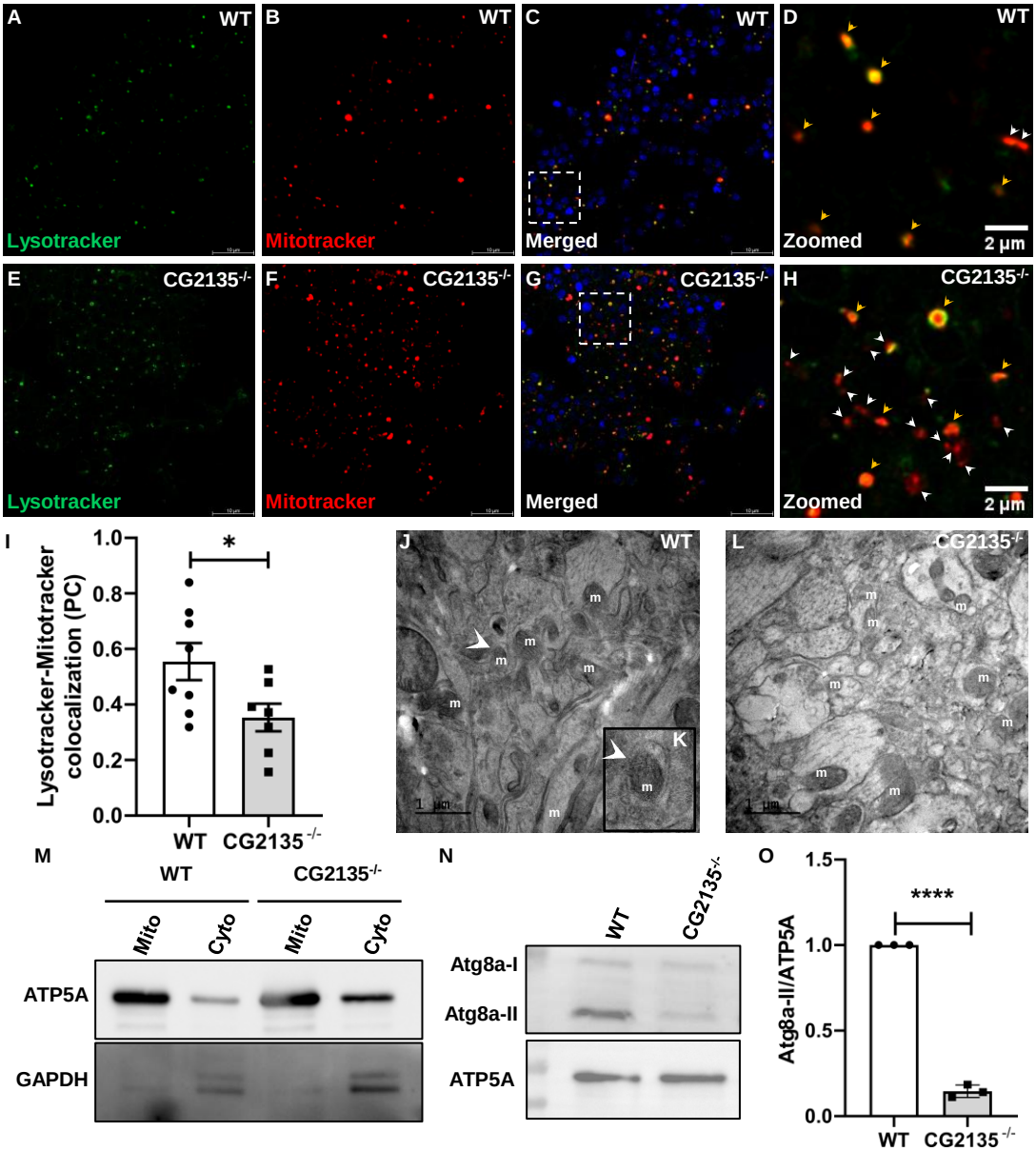

Figure 4: Impaired mitophagy in the CG2135$^{-/-}$ fly brain

(A-H) MitoTracker-LysoTracker co-staining of 45 days old wild type (WT) and CG2135$^{-/-}$ fly brain (optic lobe region) showing fewer colocalization spots (yellow puncta, indicated with yellow arrows) in the CG2135$^{-/-}$ fly, indicating reduced mitophagy. Only MitoTracker positive red puncta are indicated with white arrows. Hoechst is (blue) used for counterstaining the nucleus.

(I) Pearsons' colocalization coefficient (PCC) analysis showing reduced LysoTracker-MitoTracker colocalization in the CG2135$^{-/-}$ brain compared to WT ($N \geq 7$).

(J-L) Electron micrograph of 45 days old WT and CG2135$^{-/-}$ fly brains showing reduced mitochondria-sequestered autophagy vesicle (K) in the CG2135$^{-/-}$ fly brain as indicated by white arrow.

(M) Verification of mitochondria-rich fraction isolated from the 45 days old fly head by western blot for mitochondrial protein, ATP5A (55 kDa), and cytosolic marker GAPDH (36 kDa).

(N) The western blot with anti-Atg8a showing reduced Atg8a-II protein in the mitochondria-rich fraction from the CG2135$^{-/-}$ fly head. ATP5A was used as the loading control.

(O) The bar graph showing the quantification for the Atg8a-II/ATP5A. N=3

All experiments were done independently. Error bars represent the standard error of mean (SEM). Asterisks represent a level of significance (****$P \leq 0.0001$, *$P \leq 0.05$; Student's *t*-test).

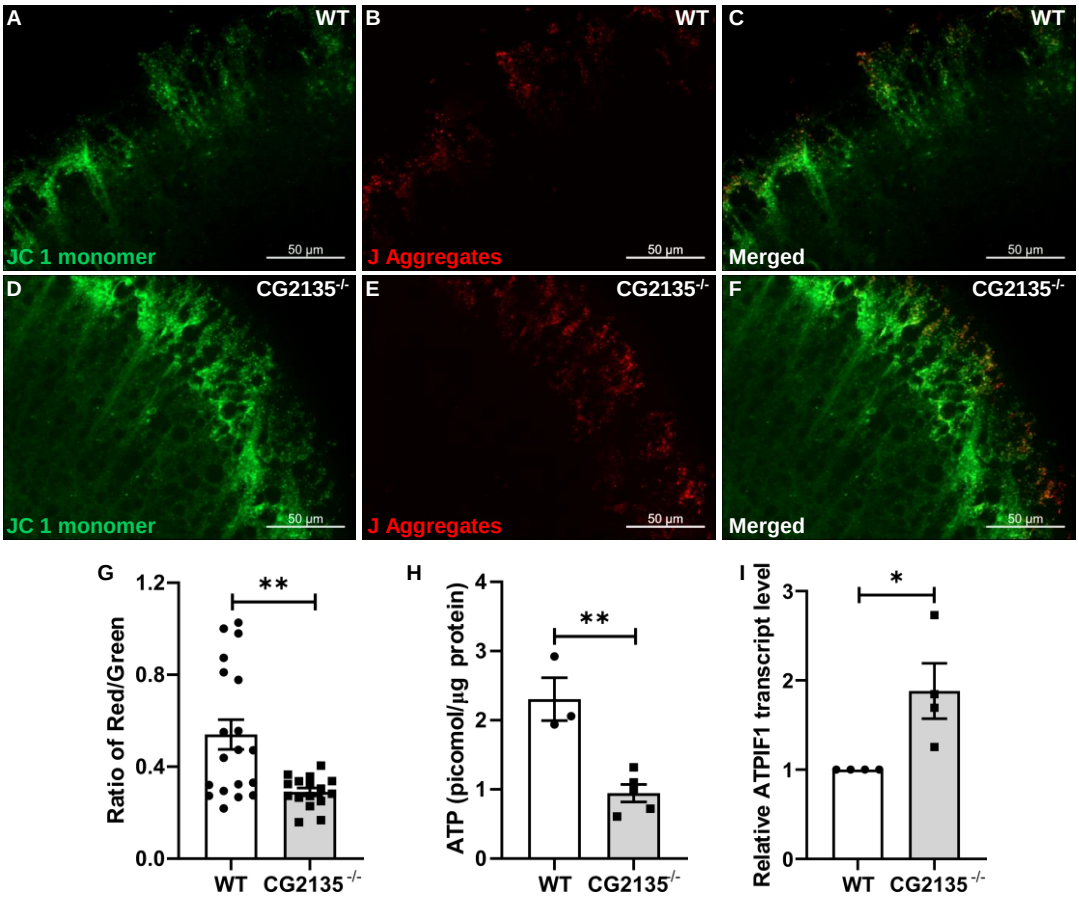

Figure 5: Reduced mitochondrial membrane potential and ATP levels in the CG2135$^{-/-}$ fly brain.

(A-F) The optic lobes of 45 days wild type (WT) and CG2135$^{-/-}$ fly brains were stained with JC-1 dye for assessing the mitochondrial membrane potential ($\Delta\Psi m$).

(G) The bar graph represents quantification of the red/green ratio showing reduced $\Delta\Psi m$ in CG2135$^{-/-}$ brain ($N \geq 16$)

(H) The bar graph represents quantification of total ATP from 45-days old fly head ($N = 3$), showing significantly reduced ATP levels in the CG2135$^{-/-}$ fly brains.

(I) Relative transcript levels of ATPIF1 in 45 days old CG2135$^{-/-}$ fly head determined by RT-qPCR and normalised to RP49 as housekeeping gene control (N=4).

All experiments were done independently. Error bars represent the standard error of mean (SEM). Asterisks represent a level of significance (**$P \leq 0.01$, *$P \leq 0.05$; Student's *t*-test).

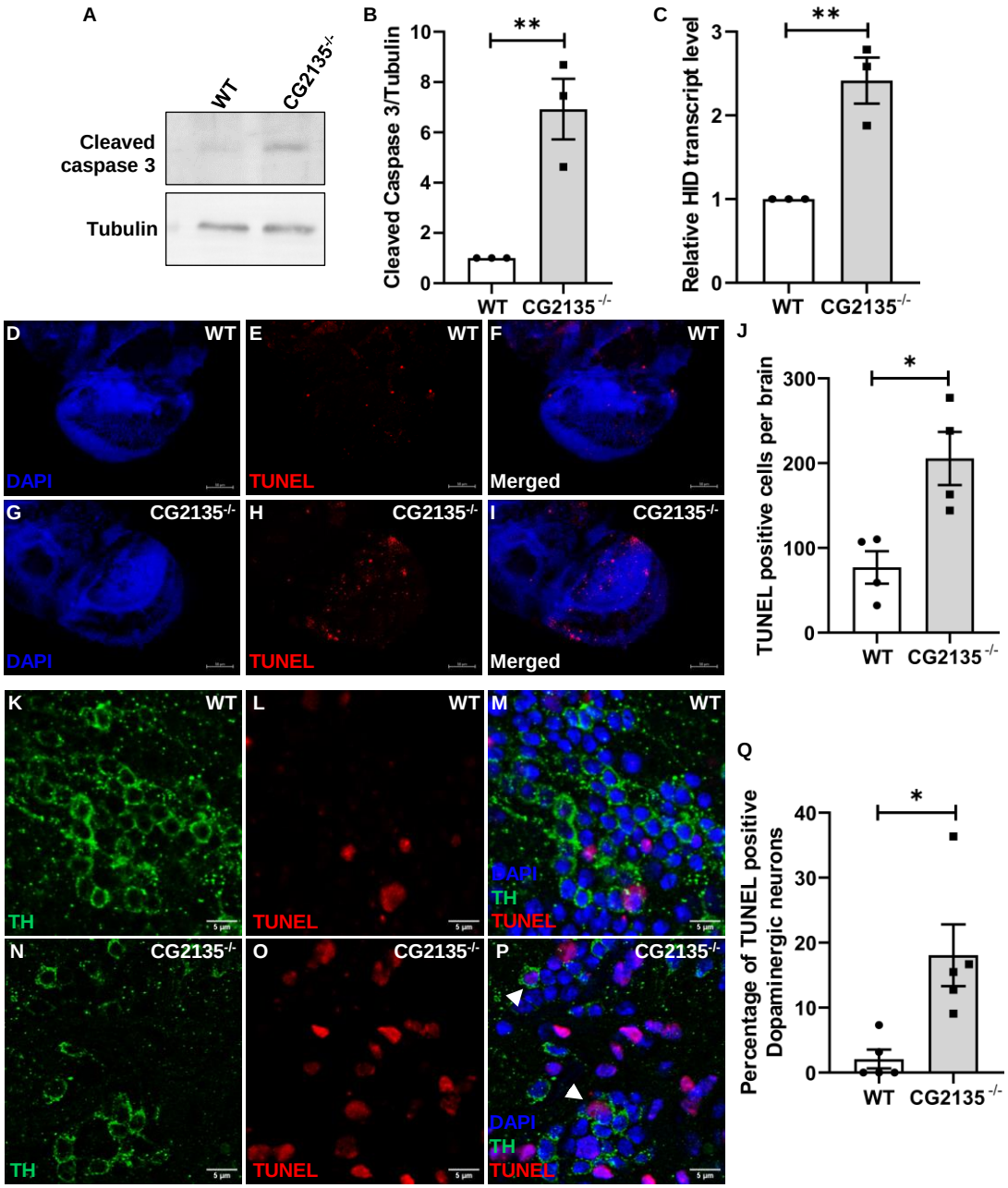

Figure 6: Increased apoptosis in the CG2135$^{-/-}$ fly brain.

(A) Western blot of Cleaved-caspase 3 using anti-Cleaved-caspase 3 antibody showing increased processed form of 22 kDa at 45 days old CG2135$^{-/-}$ fly head compared to the wild type (WT). α-Tubulin (54 kDa) was used as the loading control.

(B) The bar graph showing the relative level of Cleaved-caspase 3/Tubulin. N=3

(C) Relative transcript level of pro-apoptotic gene Hid determined by RT-qPCR and normalised to RP49 as housekeeping gene control (N=3)

(D) TUNEL staining of 45 days old WT and CG2135$^{-/-}$ brain, DAPI (blue) used for marking the nucleus.

(J) The bar graph showing quantification of the TUNEL-positive nucleus showing increased TUNEL-positive cells in CG2135$^{-/-}$ fly brain. (N=4 fly brain)

(K-P) Co-staining of TUNEL and anti-TH (tyrosine hydroxylase) showing elevated TUNEL-positive dopaminergic neurons in 45 days old CG2135$^{-/-}$ brain. DAPI (blue) was used for counter-staining the nucleus.

(Q) The bar graph representing quantification of apoptotic dopaminergic neurons (TUNEL and TH double positive) in WT and CG2135$^{-/-}$. (N=5)

All experiments were done independently. Error bars represent the standard error of mean (SEM). Asterisks represent level of significance (**$P \leq 0.01$, *$P \leq 0.05$; Student's *t*-test).

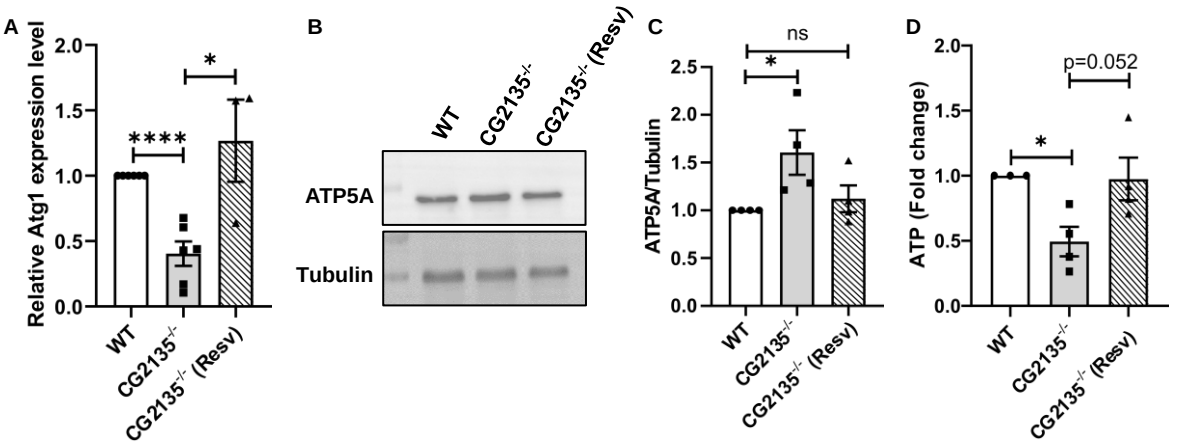

Figure 7: Resveratrol treatment corrects mitophagy defect and prevents ATP loss in the CG2135$^{-/-}$ fly brain.

(A) The bar graph represents the Atg1 transcript level determined by RT-qPCR in 30 days old wild type (WT), CG2135$^{-/-}$ and resveratrol-treated CG2135$^{-/-}$ fly head showing restoration of Atg1 level on resveratrol treatment. The gene expression was normalised to RP49 as housekeeping gene control. (N=6 for untreated WT and CG2135$^{-/-}$; N=3 for resveratrol treated CG2135$^{-/-}$).

(B) Western blot of ATP5A using anti-ATP5A antibody showing restoration of the protein level in the head lysate of CG2135$^{-/-}$ fly compared to untreated WT and CG2135$^{-/-}$ at 45 days.

(C) The bar graph showing quantification of ATP5A/Tubulin protein level in untreated WT, CG2135$^{-/-}$ and resveratrol-treated CG2135$^{-/-}$ fly head. (N=4).

(D) The bar graph represents the ATP level of WT, CG2135$^{-/-}$ and resveratrol-treated CG2135$^{-/-}$ fly head at 45 days. ATP level in CG2135$^{-/-}$ fly head restored to normalcy with resveratrol treatment. (N $\geq$ 3)

All experiments were done independently. Error bars represent the standard error of mean (SEM). Asterisks represent a level of significance (****$P \leq 0.0001$, ***$P \leq 0.001$, *$P \leq 0.05$; Student's *t*-test).

Supplementary information

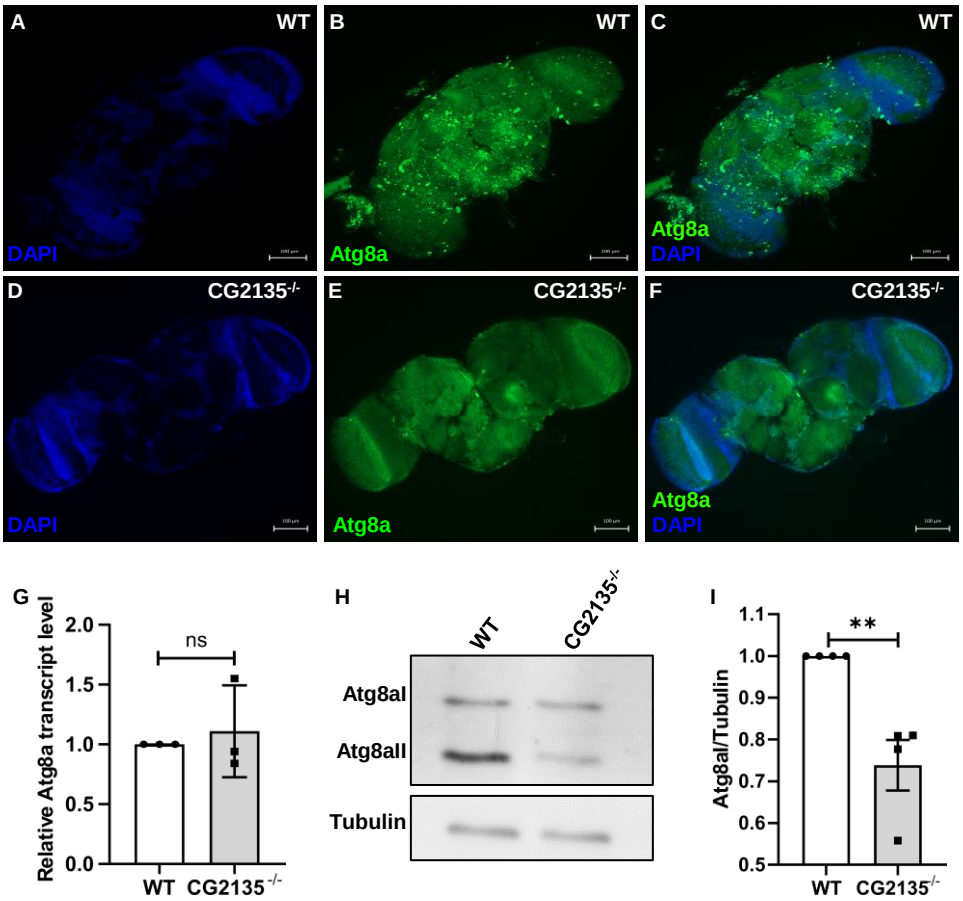

Figure S1: Reduced Atg8a in 30 days old CG2135$^{-/-}$ fly brain, Related to Figure 2

(A-F) The whole brain of 30 days WT and CG2135$^{-/-}$ was stained with anti-Atg8a (green) and counterstained with DAPI (blue), showing a low Atg8a signal in CG2135$^{-/-}$ brain compared to WT. Images taken in Apotome.2 (Carl Zeiss) and the tiles were reconstructed using Zen software. Scale bar represents 100µm.

(G) The bar graph represents the Atg8a transcript level in 30 days WT and CG2135$^{-/-}$ determined by RT-qPCR normalised to RP49 as housekeeping gene control. (N=3)

(H-I) Immunoblot of Atg8a for 30-day-old head lysate of WT and CG2135$^{-/-}$. Relative quantification of Atg8a-I/Tubulin intensity from immunoblot and tubulin kept as a loading control. (N=3)

All experiments were done independently. Error bars represent the standard error of the mean (SEM). Asterisks represent a level of significance (**$P \leq 0.01$, Student's *t*-test).

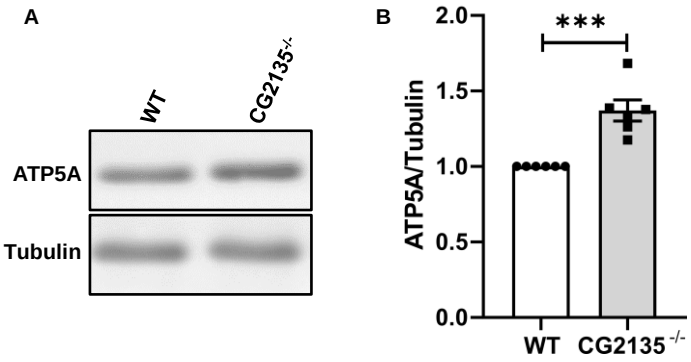

Figure S2: Western blot analysis of ATP5A protein, Related to Figure 3

(A-B) Western blot of mitochondrial protein ATP5A followed by quantification of the data shows an increased abundance of ATP5A in ≥30 days CG2135$^{-/-}$ fly brain sample, suggesting increased accumulation of mitochondria. (N=6)

All experiments were done independently. Error bars represent the standard error of mean (SEM). Asterisks represent a level of significance (***$P \leq 0.001$, Student's *t*-test).

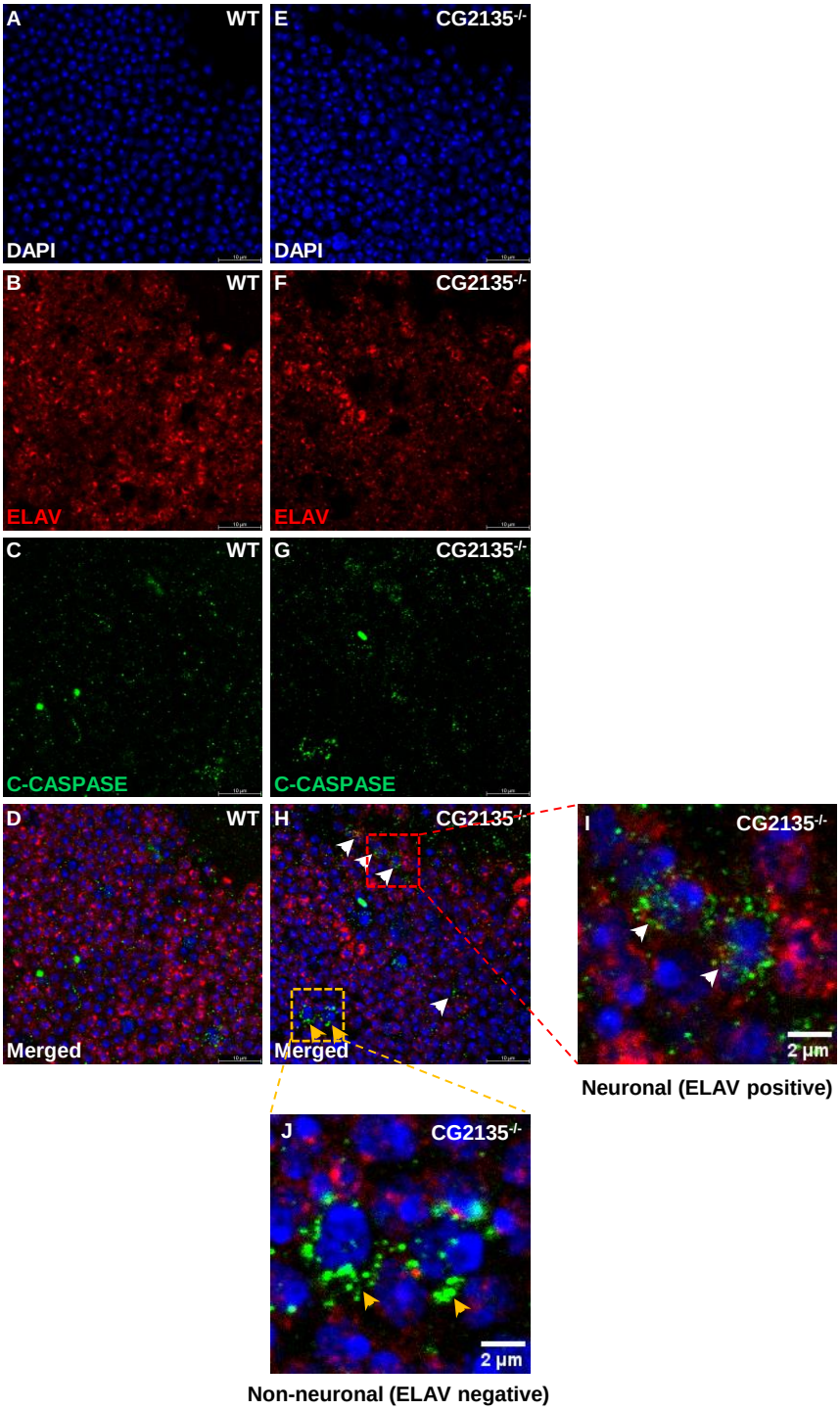

Figure S3: Accumulation of cleaved caspase3 positive cells in 45 days old CG2135$^{-/-}$ fly brain, Related to Figure 6

(A-H) Co-immunostaining with anti-Cleaved caspase 3 and anti-ELAV showed ELAV positive cells (pan-neuronal) are Cleaved caspase 3 positive cells (white arrow). A few non-ELAV cells are also Cleaved-caspase 3 positive (yellow arrow).

(I-J) Zoomed image showing ELAV positive (white arrow) pan-neuronal as well as non-Elav (yellow arrow) cells are cleaved caspase 3 positive suggesting a global apoptosis activation.